Catestatin (CST) is a key mediator of the immunoendocrine regulation of cardiovascular function

Wei Ying[2*], Kechun Tang[1*], Ennio Avolio[2], Jan M. Schilling[1,3*], Teresa Pasqua[2], Matthew A. Liu[2], Sumana Mahata[2], Gautam Bandyopadhyay[2], Soumita Das[4], Debashis Sahoo[5,6,] Nicholas J.G. Webster[1,3], Hemal H. Patel[1,3] Pradipta Ghosh[1,2,7] and Sushil K. Mahata[1,2¶].

[1]*VA San Diego Healthcare System, 3350 La Jolla Village Drive, San Diego, CA, USA*

[2]*Department of Medicine, University of California San Diego, La Jolla, CA, USA,*

[3]*Department of Anesthesiology, University of California San Diego, La Jolla, CA, USA,*

[4]*Department of Pathology, University of California San Diego, La Jolla, CA, USA,*

[5]*Department of Pediatrics, University of California San Diego, CA, USA,*

[6]*Department of Computer Science and Engineering, Jacob's School of Engineering, University of California San Diego, La Jolla, USA,*

[7]*Department of Cellular and Molecular Medicine, University of California San Diego, La Jolla, CA, USA.*

*Contributed equally to this work.

¶Correspondence should be addressed to: Sushil K. Mahata, Metabolic Physiology & Ultrastructural Biology Laboratory, Department of Medicine, University of California San Diego, 9500 Gilman Drive, La Jolla, CA 92093-0732, smahata@health.ucsd.edu.

Abstract

Objective: Hypertension (HTN) is a global pandemic, affecting more than one billion people. Although catestatin (CST), a chromogranin A (CgA)-derived peptide, decreases blood pressure (BP) in rodent models of HTN, the mechanisms underlying its hypotensive action is yet to be established. Here we generated CST knockout (CST-KO) mice to pinpoint the mechanism of the hypotensive action of CST.

Methods and Results: CST-KO mice were hypertensive; their serum cytokines were elevated, anti-inflammatory genes were downregulated, and their hearts showed marked infiltration with macrophages. CST replenishment reversed all these phenotypes - it normalized BP, reduced serum cytokines, upregulated anti-inflammatory genes, and reduced the cardiac infiltrates by ~30%, as determined by FACS. Pre-conditioning-induced cardioprotection was also abolished in CST-KO mice. We hypothesize that CST's anti-hypertensive and cardioprotective effects may be caused by suppressed trafficking of macrophages to the heart and reduced inflammation. Such *cause-and-effect* relationship is supported by the fact that CST-KO mice became normotensive when they were depleted of macrophages using chlodronate, or when they received bone marrow transplant from wild-type littermates. Mechanistically, cardiac tissue transcriptomes revealed multiple altered gene expression programs in CST-KO mice that are commonly encountered in human cardiomyopathies. Among others, a prominent reduction of *Glo1* gene was seen in CST-KO mice; supplementation with CST increased it expression by >7-fold. Because *Glo*1 in macrophages metabolizes methylglyoxal, an inflammatory agent whose accumulation promotes vascular damage in HTN and T2DM, this could be one of the means by which CST attenuates inflammation and improves cardiovascular health. Repletion of CST also improved glucose metabolism and increased the surface area of mitochondrial cristae and decreased the secretion of catecholamines; the latter explains the anti-hypertensive actions of CST.

Conclusions: We conclude that the anti-hypertensive effects of CST is mediated at least in part via CST's anti-inflammatory actions; in the absence of CST, macrophages are more reactive, they infiltrate the heart and alter the ultrastructure, physiologic and molecular makeup of the myocardium. These studies implicate CST as a key mediator of the observed crosstalk between systemic and cardiac inflammation in HTN.

Abbreviations

2DG: 2-deoxy-glucose
Actc1: cardiac muscle actin alpha
Atp5j: mitochondrial ATP synthase subunit F6
BRS: baroreflex sensitivity
Cd36: cluster of differentiation 36
Cers2: ceramide synthase 2
CgA: chromogranin A
CST: catestatin
CST-KO: CST knockout
DCM: diabetic cardiomyopathy
ER: endoplasmic reticulum
FA: fatty acid
FRT: Flp recognition target
G6P: glucose-6-phosphate
Glut4: glucose transporter 4
GO: gene ontology
GSK-3b: glycogen synthase kinase-3 beta
HCM: hypertrophic cardiomyopathy
HRV: heart rate variability
IFM: inter/intramyofibrillar mitochondria
IPC: ischemic preconditioning
LVDP: left ventricular developed pressure
LVEDP: left ventricular end diastolic pressure
Myl4: myosin light chain 4
Myl7: myosin light chain 7
mPTP: mitochondrial permeability transition pore
Myh7: myosin heavy chain 7
NADH: nicotinamide adenine dinucleotide hydride
NCD: normal chow diet
Pdk2: pyruvate dehydrogenase kinase 2
Pfkm: phosphofructokinase, muscle form
PI3K: phosphoinositide 3-kinase
PINK1: PTEN-induced putative kinase 1
Ppara: peroxisome proliferator-activated receptor alpha
qPCR: quantitative polymerase chain reaction
SBP: systolic blood pressure
Sdhc: succinate dehydrogenase complex subunit c
Slc27a1: solute carrier family 27 member 1
Slc27a2: solute carrier family 27 member 2
Sptlc1: serine palmitoyltransferase long-chain base subunit 1
SSM: subsarcolemmal mitochondria
T2DM: Type 2 diabetes mellitus
TCA: trichloroacetic acid
TEM: transmission electron microscopy
Tnni3: cardiac Troponin I
Tnnt2: cardiac Troponin T2
Tpm: tropomyosin
Ttn: Titin

Introduction

Hypertension (HTN) is an important risk factor for cardiovascular disease (CVD) and mortality [1]. The burden of HTN and the estimated HTN-associated deaths have increased substantially over the past 25 years [2].

The role of catecholamines (CAs), e.g., dopamine (DA), norepinephrine (NE), and epinephrine (Epi) in the regulation of blood pressure (BP) and their dysregulated secretion or function in HTN has been well recognized [3-7]. These CAs are produced and secreted by neuroendocrine cells e.g., chromaffin cells in the adrenal medulla and have dual hormone and neurotransmitter functions. Once released, CAs interact with numerous adrenergic receptors in a variety of tissues to impose an intricate neuro-hormonal regulation of BP.

Besides the CAs, the immune system is also recognized for its role in the genesis and progression of HTN[8-11]. Inflammation is an essential component of many diseases, and the connections between innate and adaptive immunity, HTN, and CVD add support to the role of the immune system in cardiovascular pathology [11, 12]. Known as integrators of neural, hormonal, and immune signals, it has been shown that inflammation influences CA biosynthesis by adrenal medullary cells. The converse, i.e., how CAs may impact inflammation remains unknown. More specifically, although the impact of immune activation and inflammation in the regulation of HTN is evolving, the specific immunologic mechanisms that contribute to the pathogenesis of HTN are incompletely understood. Here we reveal an unexpected role of how the process of CA secretion and its impact on systemic HTN is fueled by an immunologic phenomenon *via* Chromogranin A (CgA), and more specifically, its proteolytic biologic fragment, catestatin (CST: $hCgA_{352-372}$) [13].

Co-stored and co-released with Cas, CgA, a ~49 kDa secretory proprotein [14-16] is overexpressed in humans with essential HTN [17, 18] and in rodent genetic models of HTN [19]. Unlike CgA, plasma CST levels are diminished not only in essential HTN [18, 20] but also in the normotensive offspring of patients with HTN [20]. Additionally, HTN-associated SNPs within the CST segment of CgA have been extensively evaluated [21-28]. Processing of CgA to CST is low in patients with HTN and heart failure [18, 29], suggesting dysregulation in the processing of CgA to CST in CVD. Furthermore, both CgA heterozygote (CgA+/-) and CgA knockout (CgA-/-) mice are hypertensive [30]; but treatment with CST decreases BP and the levels of plasma CAs to that seen in control littermates. Although these findings, especially the repletion studies, point to the importance of CST and its sufficiency in reversing HTN, none conclusively show that CST is necessary. This is because CgA has many biologically active peptides, and it is possible that any or many of these CgA-derived peptides could be confounding the findings in these studies.

156 To mitigate these issues, and pinpoint the actions of CST, we generated a precise tool,
157 i.e., CST-KO mice. Given the hypertensive, hyperadrenergic, and inflammatory phenotypes in
158 these mice, we used that as a model to dissect the role of CST in the maintenance of
159 cardiovascular homeostasis. Our studies revealed a complex interplay between a trifecta: the
160 innate immune system, CA secretion from chromaffin cells in the adrenal medulla, and the
161 cardiovascular system, all coordinated by CST.
162
163

Material and Methods

Mice. To generate CST-KO mice, we selectively targeted to eliminate the 63 bp CST encoding segment from Exon VII of the *Chga* gene. The general cloning strategy involved PCR and subcloning into pBluescript. We introduced a diphtheria toxin sequence to serve as a negative selection at the 3'-end of the construct that would enrich (by ~5-fold) positive clones after transfection of the targeted construct into ES cells by electroporation. For positive selection by G418 we have introduced a Neo cassette flanked by FRT (*Flp* recognition target) site. PCR screening of CST-KO mice are shown in **Fig. S1.**

Male WT and CST-KO (20-24 weeks old) with a mixed genetic background (50% 129svJ/50% C57BL/6) were studied. Mice were kept in a 12 hr dark/light cycle and fed a normal chow diet (NCD: 13.5% calorie from fat; LabDiet 5001, Lab Supply, Fort Worth, TX). All studies with mice were approved by the UCSD and Veteran Affairs San Diego Institutional Animal Care and Use Committees (IACUC) and conform to relevant National Institutes of Health guidelines.

Protein analysis by immunobloting. Left ventricles were homogenized in a buffer containing phosphatase and protease inhibitors, as previously described [31]. Homogenates were subjected to SDS-PAGE and immunoblotted. Primary antibodies for phosphorylated and total AKT and GSK-3β were from Cell Signaling Technology; mouse monoclonal mAb 5A8 ($hCgA_{R47-L57}$) antibody [32] and rabbit polyclonal C-terminal CST pAb CT-CST ($hCgA_{P368-R373}$) [33] were generously provided by Angelo Corti (IRCCS San Raffaele Scientific Institute, Milan, Italy).

Determination of plasma CST. A commercial mouse EIA kit (RayBiotech Life, GA) was used to determine plasma CST and followed according to the manufacturer's protocol.

Non-invasive tail-cuff measurement of blood pressure. Systolic blood pressure (SBP) was measured using the mouse and rat tail cuff blood pressure (MRBP) System (IITC Life Sciences Inc. Woodland Hills, CA). Mice were restrained in plexiglass tubes and heated to 34°C for 10-15 min in individual warming chambers prior to BP measurement. The tails were placed inside inflatable cuffs with a photoelectric sensor that measured tail pulses. The SBP was measured over 6 separate days with an average of two values per day.

Measurement of plasma cytokines. Plasma cytokines were measured using U-PLEX mouse cytokine assay kit (Meso Scale Diagnostics, Rockville, MD) via the manufacturer's protocol.

198

199 **Real Time PCR**

200 Total RNA from heart tissue was isolated using RNeasy Mini Kit and reverse-transcribed using
201 qScript cDNA synthesis kit. cDNA samples were amplified using PERFECTA SYBR FASTMIX L-
202 ROX 1250 and analyzed on an Applied Biosystems 7500 Fast Real-Time PCR system. All PCRs
203 were normalized to *Rplp0*, and relative expression levels were determined by the $\Delta\Delta C_t$ method.

204

205 **Flow cytometry analysis**

206 Mouse heart perfusion was performed as previously described [34]. Cardiac stromal cells were
207 stained with fluorescence-tagged antibodies to detect macrophages ($CD11b^+F4/80^+$). Data were
208 analyzed using FlowJo software.

209

210 **Tissue macrophage depletion study.**

211 To deplete tissue macrophages, mice were given clodronate liposomes (50 mg/kg body weight;
212 catalog F70101C-N, FormuMax, Sunnyvale, CA) every 3 days via intraperitoneal injection. Mice
213 treated with control liposomes were used as control.

214

215 **Bone marrow transplantation.**

216 To generate irradiated chimeras, 10-12 weeks old WT or CST-KO NCD recipient mice received
217 a lethal dose of 10 Gy radiation, followed by tail vein injection of 2 x 10^6 bone marrow cells from
218 either WT or CST-KO NCD donor mice. After 16 weeks of bone marrow transplantation, all mice
219 were subjected to non-invasive tail-cuff measurement of BP.

220

221 **Transmission Electron Microscopy (TEM) and morphometric analysis.** To displace blood
222 and wash tissues before fixation, mice were cannulated through the apex of the heart and
223 perfused with a Ca^{2+} and Mg^{2+} free buffer composed of DPBS, and 9.46 mM KCl (to arrest hearts
224 in diastole), as described previously [35]. Fixation, embedding, sectioning and staining were done
225 following our previous publication [35]. Grids were viewed using a JEOL JEM1400-plus TEM (JEOL,
226 Peabody, MA) and photographed using a Gatan OneView digital camera with 4k x 4k resolution
227 (Gatan, Pleasanton, CA). Morphometric analysis of glycogen granules and cristae surface area
228 were determined as described previously by us [35].

229

230 **Microarrays.** Total RNA from left ventricular tissue from four CST-KO and age-matched WT mice
231 was isolated using a RNeasy Kit. RNA quality was assessed by using the Agilent Model 2100

Bioanalyzer. RNA was labeled and hybridized to a Nimblegen mouse 12-plex array. Array was scanned on a GenePix 4000B scanner and data extracted using Arraystar 4. Raw data was analyzed using a Bayesian variance modeling approach in VAMPIRE using a FDR of 0.05 [36]. Data were visualized using GeneSpring 14.5. Microarray data is available at GEO Accession Number (GSE104071).

***In vivo* tissue glucose uptake and metabolism.** *In vivo* glucose uptake and production of glucose-6-phosphate (G6P) and glycogen was assessed following a published protocol but using double isotopes - ^{3}H-glucose and ^{14}C-2-deoxyglucose (2DG) as described previously by us [35].

***In vivo* fatty acid incorporation and lipid extraction and oxidation.** A 100 µl solution of U-^{14}C-palmitic acid-BSA complex (molar ration 2.5:1), containing 1 µCi and 250 µM palmitate was injected per mouse. After 90 min, mice were sacrificed, blood was saved and tissues were subjected to lipid extraction by Bligh and Dyer's adaptation [37] of Folch's original method [38]. Radioactivity in the lower chloroform layer was determined by measuring fatty acids in the aqueous layer by determining acid soluble metabolites (ASM, representing fatty acid oxidation) as described previously by us [39].

Determination of tissue glycogen. Glycogen was extracted from the left ventricle by boiling with 30% KOH, precipitation by alcohol and determination with anthrone reagent [40].

Langendorff perfused heart model. Mice were anesthetized with sodium pentobarbital (50 mg/kg i.p.), the heart was excised and the aorta was cannulated for Langendorff perfusion of the coronary circulation, as described previously [41]. For the ischemic preconditioning (IPC) protocol the stabilization period was followed by two cycles of ischemia (5 min, no pacing) and reperfusion (5 min, pacing after 1 min re-perfusion).

Measurement of catecholamines: Mice were anesthetized by inhalation of isoflurane and blood was collected from the heart in potassium-EDTA tubes. Adrenal and plasma catecholamine were measured using 3-CAT Research ELISA kit (LDN Immunoassays and Services, Nordhorn, Germany).

Statistics. Statistics were performed with SPSS Statistics (IBM Corp., Armonk, NY). Data were analyzed either with a Repeated Measure (RM) 2x2 ANOVA, 2-way ANOVA, UNIANOVA, and

266 subjected to post-hoc tests and pairwise comparisons where appropriate. Additionally, we
267 performed unpaired student's t-test or Mann-Whitney U test depending on Shapiro-Wilk's test of
268 normality (with results corrected for Levene's test for Equality of Variances where appropriate).
269 All data are presented as mean ± SEM and significance was assumed when $p<0.05$.
270

Results

Generation and validation of CST-KO mice. Our strategy (see **Fig 1; S1**) for the development of CST-KO mice involved a targeted elimination of the CST domain (63 bp) from Exon VII of the *Chga* gene. CST-KO mice were expected to express truncated CgA but not CST. We confirmed this by western blot analyses of lysates prepared from adrenal glands. The presence of CgA was confirmed using a mouse monoclonal antibody (mAb 5A8) [32] (**Fig. 1B**) and a CgA ELISA (**Fig. 1D**); however, blots using a polyclonal antibody directed against the 6 C-terminal domains of CST (pAb CT-CST) [33] showed a proteolytically processed CgA of ~46 kDa corresponding to $mCgA_{1-385}$ in WT littermates, but not in CST-KO mice (**Fig. 1C**). Because this antibody detected synthetic CST (a positive control, indicating specificity of the antibody) we conclude that CST-KO mice indeed lack CST (**Fig. 1C**). Analyses of levels of CST in the plasma from these mice further confirmed the complete absence of CST in CST-KO mice (**Fig. 1E**).

CST-KO mice are hypertensive and have enlarged and inflamed hearts; key phenotypes are reversed by supplementation with recombinant CST. We checked several cardiovascular parameters that are expected to be affected by the lack of CST. We found that CST-KO hearts are ~27% heavier than WT mice (**Fig. 1F&G**) and that the mice are hypertensive (**Fig. 1H**). These findings indicate that heart structure and function are regulated by CST.

Next, we checked plasma CST level before and after treatment with exogenous recombinant CST. In WT mice, plasma CST level was 0.86 nM, which increased to 1.72 nM 24 hr after treatment with exogenous CST (**Fig. 2B**). In CST-KO mice, plasma level of CST was undetectable at baseline, as expected, and rose to 1.17 nM after supplementation (**Fig. 2B**). These findings indicate that the supplementation of CST-KO mice with CST provides near physiological concentration of CST. Through a series of studies, we next examined the phenotypes of CST-KO mice and asked whether CST supplementation can restore some of the key phenotypes.

First, we found that CST-KO mice show increased levels of proinflammatory plasma cytokines including TNFα, IFNγ, MIP1α, MCP1, and KC/GRO (**Fig. 2C**). By contrast, anti-inflammatory cytokine IL10 is decreased in CST-KO mice (**Fig. 2C**). CST treatment decreased plasma proinflammatory cytokines and increased anti-inflammatory IL10 in both WT and CST-KO mice (**Fig. 2C**). These findings in plasma cytokine levels were consistent with transcripts in the heart muscle, as determined by qPCR-- CST-KO mice showed a reduction in several anti-inflammatory markers (*IL4*, *Arg1*, *Clec7a* and *Clec10a*) (**Fig. 2D**) and a concomitant increase in several other pro-inflammatory markers (**Fig. 2E**). These findings show that the balance between

pro- and anti- inflammatory pathways was skewed towards inflammation in CST-KO mice. Exogenous CST supplementation reversed this disbalance; it induced several anti-inflammatory pathways (**Fig. 2D**) and either normalized or markedly decreased proinflammatory cytokine mRNA levels (**Fig. 2E**). These findings in the heart muscle and the plasma show that CST is both necessary and sufficient for restoring immune homeostasis in the heart and in the systemic circulation, respectively. The findings are also in accordance with CST's role as an anti-inflammatory peptide [42-45].

Second, we checked the systolic BP (SBP) in these mice: High BP in CST-KO mice was reduced to WT level after supplementation with CST (**Fig. 3A-B**). These findings demonstrate that CST is necessary and sufficient for BP homeostasis and are consistent with the previously described anti-HTN functions of CST [30, 46]. In addition, the finding that CST-KO mice display a proinflammatory hypertensive phenotype is also consistent with prior studies showing that proinflammatory cytokines (IL6) increase BP [47-49] and anti-inflammatory cytokines (IL2 and IL10) decrease BP [50 51-54].

Third, we analyzed the microarchitecture of the heart: In the saline-treated WT mice, Transmission Electron Microscopic (TEM) micrographs showed resident macrophages in the inter-sarcolemmal spaces (**Fig. 3C**). In contrast, the saline-treated CST-KO heart showed a marked infiltration of monocyte-derived macrophages (**Fig. 3C**), indicating inflammation of the CST-KO heart. While treatment of WT mice with CST did not change the resident macrophage population, CST-KO mice showed almost complete disappearance of infiltrated macrophages after CST substitution (**Fig. 3F**). This was supported by FACS analysis showing ~38% decrease of $CD11b^{+}F4/80^{+}$ macrophages in CST-supplemented CST-KO heart (**Fig. 3D**). These findings reveal that CST is required for cardiac homeostasis and its absence is permissive to cardiac inflammation.

Macrophages are key effector cells responsible for the anti-inflammatory actions of CST. Next, we explored the implications of infiltrated macrophages in the hearts of CST-KO mice and its relevance to cardiovascular physiology using two independent approaches (**Fig. 3A**). First, we depleted macrophages by chlodronate (CDN) liposomes, which not only depleted resident and infiltrated macrophages but also reversed the HTN phenotype of CST-KO mice (**Fig. 3G&H; S2**). Because CDN did not reduce BP in WT mice, these findings show that macrophages may not be required for normal cardiac functions, but its dysregulation (increased infiltration and/or aberrant activation) may be a key contributor of the HTN phenotype in CST-KO mice.

Second, we carried out bone marrow transplantation (BMT) assays in which, we irradiated both WT and CST-KO mice and then cross-transplanted their marrows-- CST-KO bone marrow was transplanted into WT mice and *vice versa*. To our surprise, we found that BMT could transfer the hypertensive phenotype-- while CST-KO-marrow recipient WT mice showed increased BP, WT-marrow recipient CST-KO mice showed decreased BP (**Fig. 3I**). These findings indicate that paracrine secretion of CST and/or cytokines by macrophages may regulate BP.

To confirm if CST is responsible for the observed BMT-induced phenotype switch, we analyzed plasma CST and found that CST-KO mice who received WT-marrow, but not CST-KO-marrow had near physiologic levels of CST in their plasma (0.52 nM) (**Fig. 3J**). These findings suggest marrow-resident immune cells and/or hematopoietic system are a major contributor of circulating CST in the plasma. They may do so either directly [through paracrine secretion from macrophages, as observed in the case of serum cytokines (**Fig. 2C**)] or indirectly (perhaps *via* other immune cells that feedback and regulate macrophage response).

Regardless, our studies using CDN and BMT implicate the macrophages and the innate immune system as key effectors of the anti-hypertensive actions of CST. In the absence of CST (as in CST-KO mice), macrophages are hyperactive and support both systemic (**Fig. 2**) and local cardiovascular inflammation (**Fig. 3**) and trigger systemic HTN.

Microarray studies reveal that CST impacts core bioenergetic and metabolic functions of the myocardium. To gain insights into the nature of the immunoendocrine actions of CST on the heart, next we carried out transcriptomic analyses (gene microarray) of the left ventricles of WT and CST-KO. Analysis revealed 437 genes with altered expression, up- or downregulated (false discovery rate <0.05), as shown in the form of a heatmap (**Fig. 4A**).

Downregulated genes, which were most enriched in pathways that impact muscle conduction and contractility (**Fig. 4B**) include, among other genes, *Glo1* (encodes glyoxylase I enzyme that detoxifies methylglyoxal, which is a cytotoxic byproduct of glycolysis). Upregulated genes include, among others, *Gm7120* (encodes predicted gene 7120 that acts as a hypercapnia responsive gene), *Astn2* (encodes astrotactin 2 that functions as a lipid raft), and *Defa20* (encodes defensin α-20 that exerts antibacterial humoral response) genes.

We validated several of these up- and downregulated genes by qPCR and found that CST supplementation reversed these aberrant expressions in all cases, i.e., downregulated what was aberrantly overexpressed or upregulated what was aberrantly suppressed (**Fig. 4C**). Of note, *Glo1* in macrophages metabolizes methylglyoxal, an inflammatory agent whose accumulation promotes vascular damage in HTN and diabetes. Therefore, it is possible that CST attenuates

inflammation and improves cardiovascular health in part through the regulation of *Glo1* expression.

Targeted qPCR analyses of sarcomeric genes revealed reduced expression of *Tnni3* (encodes cardiac troponin I, which helps to coordinate the contraction of the heart), *Tnnt2* (encodes cardiac troponin T, which helps coordinate cardiac contraction), *Myl4* (encodes atrial light chain-1 and is associated with atrial fibrillation) and *Myl7* (encodes atrial light chain-2 and modulates cardiac development and contractility) genes in CST-KO mice (**Fig. 4D**). CST treatment increased expression of *Tnni3*, *Tnnt2*, *Actc1* (encodes cardiac α-actin that is a major constituent of the cardiac contractile apparatus), *Myl4* and *Myl7* genes in both WT and CST-KO mice albeit to a much higher level in CST-KO mice (**Fig. 4D**).

Tpm (encodes tropomyosin protein that binds to actin filament and regulates cardiac contraction) and *Ttn* (encodes titin protein, which interacts with actin and myosin and regulate cardiac contraction) genes were not affected by the presence or absence of CST.

An analysis of mitochondrial genes revealed reduced expression of *Ndufa3* (nuclear-encoded NADH-ubiquinone oxidoreductase 1 alpha subcomplex 3 of Complex I), *Sdhc* (nuclear-encoded succinate dehydrogenase complex subunit C that is a subunit of Complex II) and *Atp5j* (encodes mitochondrial membrane ATP synthase subunit 6 of Complex V, which produces ATP from ADP) genes in CST-KO mice (**Fig. 4E**). CST treatment increased the expression of all three genes in WT and CST-KO mice (**Fig. 4E**).

Taken together, these unbiased approaches and qPCR validation studies provide insights into how an inflamed dysfunctional heart in the absence of CST may impact some of the core fundamental functions of this vital organ by affecting its ultrastructure, muscle function (contractility), rhythm, mitochondrial bioenergetics and conduction.

CST-KO mice display a cardiometabolic shift: glucose utilization is decreased with a concomitant increase in the utilization of fatty acids and insulin resistance. We next asked how CST may impact metabolism. Prior studies have shown that the heart is an omnivore, which consumes fat, carbohydrate, protein, ketone bodies, or lactate [55], generating ~95% of total energy via oxidation of fatty acids and glucose [56, 57]. Because diabetic hearts shift away from the utilization of glucose [58], relying almost completely on fatty acids as an energy source, we looked at cardiac metabolism in CST-KO mice, which we recently reported to be insulin-resistant [42]. CST-KO mice showed decreased uptake of 2DG in LV compared to WT mice (**Fig. 5A**). Furthermore, G6P utilization was significantly lower in CST-KO compared to WT (**Fig. 5A**). No significant difference between CST-KO and WT was seen in generation of G6P (**Fig. 5A**).

We next looked at the mRNA levels of key genes involved in glucose metabolism. Thus, we found decreased mRNA expressions of *Glut4* (encodes glucose transporter 4), *Pfkm* (encodes the muscle isoform of phosphofructokinase, which catalyzes the irreversible conversion of fructose-6-phosphate to frustose-1,6-bisphosphate) and *Pdk2* (encodes pyruvate dehydrogenase protein kinase-2 that phosphorylates and inhibits pyruvate dehydrogenase activity resulting in decreased glucose utilization and increased fat metabolism) in CST-KO mice compared to WT mice (**Fig. 5B**), which corroborate with the biochemical findings.

Since plasma insulin level of CST-KO mice was higher than WT mice [42], poor glucose metabolism correlate with reduced insulin sensitivity in CST-KO mice. CST supplementation improved glucose uptake and utilization in CST-KO mice (**Fig. 5A**), indicating CST has an insulin-like activity or CST is an insulin-sensitizing peptide. We also found that compared to WT mice, CST-KO mice show a significant higher FA uptake (**Fig. 5C**). This could be due to the higher plasma insulin level in CST-KO mice [42] that drives increased lipid metabolism (but not higher glucose metabolism due to insulin resistance). Furthermore, ^{14}C-labeled acid soluble metabolites (ASM) were significantly higher in CST-KO compared to WT mice (**Fig. 5C**). These findings suggest that increased dependence on fatty acids for energy needs make CST-KO hearts resistant to insulin.

We confirmed these biochemical findings by analyzing the levels of expression of key genes involved in lipid metabolism. We found increased mRNA levels of fatty acid transporter *Cd36* (encodes cd36 antigen, which is scavenger receptor, and functions in high affinity tissue uptake of long-chain fatty acids) and *Slc27a1 (FATP1)* (encodes long-chain fatty acid transporter 1, which transports long-chain fatty acids in an ATP-dependent manner) as well as of the enzyme for triglyceride formation *Dgat2* (encodes diacylglycerol O-acyltransferase 2 enzyme, which catalyzes the terminal step in triacylglycerol synthesis), and the transcription factor *Pparα,* which supports fatty acid oxidation (**Fig. 5D**). In addition, we found increased expression of *Sptlc1* (encodes serine palmitoyltransferase enzyme, which catalyzes the 1st step in sphingolipid biosynthesis) and *Cers2* (encodes ceramide synthase 2 enzyme, which catalyzes the synthesis of very long acyl ceramides, including C20 and C26 ceramides) genes (**Fig. 5D**), indicating increased ceramide synthesis, which will make the CST-KO heart more resistant to insulin.

In contrast, CST treatment decreased expression of *Cd36*, *Dgat2*, *Sptl1c*, *Cers2* and *Ppara* (key regulator of lipid metabolism) genes. These findings indicate that CST improved metabolic health of the CST-KO heart by converting them from insulin-resistant to insulin-sensitive. Next, we checked the status of glycogen (readily mobilized storage form of glucose). We found low glycogen storage in 'Fed' CST-KO heart compared to 'Fed' WT mice. CST

supplementation improved glycogen storage in both WT and CST-KO heart (**Fig. 5E**). The biochemical findings were supported by morphometric analyses of glycogen granules in EM micrographs (**Fig. 5F&G**).

Furthermore, because increased accumulation of fatty acids, diacylglycerol, and ceramide impairs insulin signaling [59], we also evaluated the hearts from WT and CST-KO mice for phosphoproteins (e.g., AKT and GSK-3β) within the insulin signaling cascades that are commonly indicative of the metabolic effects of insulin. We found that the hearts from CST-KO mice had reduced phosphorylation of AKT at ser473 site and GSK-3β at ser9 site (**Fig. 5H-J**), indicating decreased insulin sensitivity. This phenotype was reversed upon CST treatment because both phosphoproteins were restored in the hearts of CST-KO mice (**Fig. 5H-J**). These findings reinforce CST as an insulin-sensitizing peptide in the heart, which is consistent with its previously described role in other tissues [42, 60].

Taken together with the cardiometabolic shifts, these findings indicate that CST is a hormone that maintains cardiometabolic homeostasis; it does so at least in part by acting as an insulin-sensitizing peptide which regulates myocardial choice of substrate for generating energy (i.e., ATP).

The myocardium in CST-KO mice show mitochondrial dysfunction. The myocardium relies heavily on mitochondria for the generation of ATP and maintenance of intracellular Ca^{2+} fluxes [61]. Prior studies have shown that HTN is associated with structural mitochondrial abnormalities that result in impaired energy production and accelerated formation of ROS through instability of electron transport chain complexes [62, 63]. Because the hypertensive CST-KO mice showed gene expression **(Fig. 4)** and biochemical **(Fig. 5)** profiles indicative of altered bioenergetics and mitochondrial dysfunction, next we analyzed the mitochondria health in the WT and CST-KO mice. To this end, we used TEM to analyze and resolve the two populations of mitochondria in the heart-- the interfibrillar mitochondria (IFM) which align in longitudinal rows between myofibrils and the subsarcolemmal mitochondria (SSM) that localize below the sarcolemma. These two subpopulations have distinct respiration rates associated with different metabolic enzyme activities, morphological structures, and lipid contents [64, 65]. Under low magnification we analyzed the shape, location and orientation of SSM (**Fig. 6A-D**) and IFM (**Fig. 6I-L**). Under high magnification we analyzed the shape and orientation of mitochondrial cristae [SSM (**Fig. 6E-H**) and IFM (**Fig. 6M-P**)]. These morphometric analyses revealed significant reduction in cristae surface area in CST-KO mice, which was rescued after CST supplementation (**Fig 6E-H; 6M-P**).

Because cristae shape and density determine the assembly and stability of respiratory chain supercomplexes and efficiency [63], taken together with transcriptomic and biochemical analyses the TEM findings showed that both mitochondrial structure and function are impaired in the hearts of CST-KO mice.

Consistent with myocardial insulin resistance, CST-KO hearts showed accumulation of lipid droplets, which are implicated in contractile and diastolic dysfunctions [66, 67]. Mitophagy, the mitochondrial-specific analog of autophagy, represents breakdown of damaged and malfunctioning mitochondria [68-70]. Mitophagy in CST-KO mice indicates impaired mitochondrial function. CST supplementation improved cristae surface area, markedly reduced lipid accumulation, and decreased mitophagy in CST-KO heart. These findings indicate that CST can enhance cardiovascular functions by improving the health of mitochondria, and thereby cardiomyocyte metabolism.

Ischemic pre-conditioning-induced cardioprotection is severely impaired in CST-KO heart. We investigated the response of hearts from WT and CST-KO mice to ischemia/reperfusion (I/R) and tested responses to ischemic preconditioning (IPC). For the functional measures 'LVDP (mmHg)' (**Fig. S3A**), 'LVEDP (mmHg)' (**Fig. S3C**), 'dP/dt$_{max}$ (mmHg/sec.)' (**Fig. S3B**), 'dP/dt$_{min}$ (mmHg/sec.)' (**Fig. S3D**) revealed that IPC significantly increased post-ischemic LVDP and lowered LVEDP in WT hearts compared to CST-KO hearts and their respective IR controls (**Fig S3A&3C**). Furthermore, neither LVDP nor LVEDP was significantly modified in IPC treated CST-KO hearts compared to respective IR controls. Sidak's pairwise comparison revealed that IPC improved recoveries of both dP/dt$_{max}$ (**Fig. S3C**) and dP/dt$_{min}$ (**Fig. S3D**) compared to respective IR controls. When compared to CST-KO mice, a moderate effect on dP/dt$_{max}$ and dP/dt$_{min}$ was seen (few significant time-points during 45 min reperfusion). Furthermore, neither dP/dt$_{max}$ nor dP/dt$_{min}$ was increased significantly in IPC treated CST-KO hearts compared to respective IR controls. Detailed values for pair-wise comparisons are included in a supplementary table.

In aggregate, these data show CST-KO mice could not be preconditioned to the extent seen in WT mice. WT mice were protected with IPC, with observed improvements in all functional measures in the re-perfusion period, while CST-KO mice showed only marginal improvements.

CST-KO adrenal medulla is populated with infiltrated macrophages and heightened sympathetic stimulation with consequent hypersecretion of catecholamines. Because prior studies have implicated altered CA secretion from an inflamed adrenal medulla in progression of HTN [3, 4], we next evaluated the adrenal glands in the CST-KO mice. TEM studies revealed that

compared to WT littermates, CST-KO mice had an abundance of infiltrated macrophages in the intercellular spaces of chromaffin cells (**Fig. 7A)**. Supplementation with CST reduced the abundance of macrophage infiltrates in CST-KO mice, but did not affect the resident macrophage population in the WT mice (**Fig. 7A**). By contrast, treatment with chlodronate resulted in complete loss of macrophages (both resident and infiltrates) in both WT and CST-KO mice (**Fig. 7A**).

Because prior studies in humans, mice and rats have shown that pro-inflammatory cytokines such as IFNα [71, 72], IL1β [73, 74], and TNFα[75, 76] increase CAs production and secretion, we asked if the inflamed adrenal glands in CST-KO mice produce and secrete more CAs. We found that compared to WT littermates, both adrenal (**Fig. 7B**) and plasma (**Fig. 7C**) levels were elevated in CST-KO mice. In addition, the CST-KO adrenal medulla exhibit abundant docked chromaffin granules (CG) and decreased acetylcholine containing vesicles at the sympatho-adreno-medullary synapse (**Fig. 7D&E**), implicating heightened sympathetic nerve activity eventuating in hypersecretion of CA. Supplementation of CST-KO mice with CST not only inhibited infiltration of macrophages in the adrenal medulla (**Fig. 7A**) but also had a concomitant decrease in both plasma and adrenal CAs (**Fig 7B&C**).

These findings demonstrate that CST is necessary and sufficient to suppress CA production and secretion and thereby exert its anti-HTN effect and orchestrate cardiometabolic homeostasis. Findings also support the following working model for how CST may accomplish these roles *via* two independent but synergistic mechanisms (see **Fig. 8**): (i) inhibiting the infiltration of macrophages, thereby inhibiting paracrine cytokine regulation of CA production and secretion, (ii) attenuating sympathetic nerve activity, thereby decreasing cholinergic stimulus for secretion of CA.

Discussion

Previous studies showing low levels of CST in hypertensive subjects [20] and normalization of BP in CgA-KO mice by CST [30] as well as decreasing BP in polygenic models of rodent HTN [46] indicate that CST is sufficient to reverse HTN. The findings of hypertensive phenotype in CST-KO mice and restoration of that phenotype by exogenous administration of recombinant CST establishes that CST is both necessary and sufficient in regulating HTN. This precise experimental model also uncovered three mutually interdependent mechanisms (discussed below) *via* which CST may exert its anti-HTN and cardioprotective effects, and thereby, maintain cardiovascular homeostasis.

Immunoendocrine regulation of BP. Cardiac macrophages are critical for myocardial homeostasis [77-81]: while a subset of them orchestrate monocyte recruitment and contribute to heart failure pathogenesis [82], another is increased during diastolic dysfunction [34], myocardial infarction and acute hemodynamic stress [77, 83]. We found an abundance of infiltrated macrophages in the hearts and the adrenal glands of CST-KO mice. Using two parallel approaches (chlodronate and BMT) to decrease macrophage activity, we found that macrophages are key effector cells for the anti-HTN actions of CST.

Immune regulation of cardiometabolic homeostasis, mitochondrial structure and function. The regulation of heart function by immune cells is well documented [84, 85]. Although myocardial dysfunctions in rodents[86] and humans [87, 88] have been associated with increased TNFα production, how inflammation may reduce cardiac contractility and/or conduction, two of the most important functions of the myocardium, remains poorly defined. Contractility of the myocardium requires ATP [89], ~6 kg of ATP/ d, which is ~20 times its own weight [90-93], produced predominantly *via* oxidative phosphorylation in the mitochondria and, to a lesser extent, by glycolysis [94]. Therefore, mitochondrial health is critical for the proper functioning of the heart. A plethora of substrate are used to produce ATP, including fatty acids, glucose, some amino acids, lactate, and ketones [55, 95] and substrate selection depends largely on substrate availability, oxygen concentration and myocardial workload [96, 97]. Under normal conditions, the heart relies predominantly (~60-90%) on fatty acid (FA) oxidation to fuel ATP production, whereas the remaining ~10-40% of ATP is derived from pyruvate oxidation [98]. Metabolic flexibility (the capacity of the healthy heart to shift between different substrates to ensure a continuous output of energy) is established as a crucial feature of cardiac energy metabolism [99]. Such flexibility was lost in

CST-KO mice because hearts in these mice showed increased FA uptake and oxidation coupled with decreased glucose uptake and oxidation in CST-KO mice; these changes have been reported in insulin-resistant and diabetic rodents [100-102] and is a distinctive feature in obesity-associated metabolic diseases in humans [103-105]. Such metabolic inflexibility, was reversed by supplementation of CST-KO mice with CST, underscoring that CST is necessary and sufficient for cardiometabolic homeostasis and flexibility.

As for how CST may regulate the cardiometabolic state, we found that mitochondrial structure and function were altered in its absence and restored by exogenous supplementation of CST. These findings are consistent with prior studies showing that HTN is associated with decreased mitochondrial mass and density, increased mitochondrial swelling, impaired energy production and the accelerated formation of reactive oxygen species (ROS) [62]. In addition, HTN rats display mitochondrial fragmentation and increased ROS production [106].

In congruence with increased FA uptake in the setting of decreased mitochondrial oxidative capacity, CST-KO mice displayed intramyocardial lipid droplets; such droplets are normally found in an obese and diabetic heart [107-109] and are known to trigger mitochondrial dysfunction and energetic compromise eventuating in cardiac dysfunctions [104, 110, 111]. In addition, like a diabetic heart, myocardial insulin resistance (decreased phosphorylation of AKT and GSK-3β) and impaired glucose utilization (decreased glucose uptake and oxidation) in CST-KO mice resulted in a further increase in cardiac FA uptake and accumulation of toxic lipid metabolites including triacylglycerol, diacylglycerol and ceramide [112-114]. Of note, inflammatory cytokines like TNFα induces synthesis of ceramides, linking immune cells in induction of ceramide synthesis [115]. We have previously shown that CST markedly decreases triglyceride, FA and ceramides in diet-induced obese (DIO) liver and improves insulin sensitivity in CST-KO and DIO mice [42]. CST supplementation in CST-KO mice results in the development of the following phenotypes: (i) increased glucose uptake and metabolism, (ii) decreased FA uptake and oxidation, (iii) decreased accumulation of lipid droplets, and finally, (iv) decreased mitophagy. These findings underscore the crucial roles that CST plays in improvement of cardiac metabolism and function.

Neuro-adrenergic overdrive-induced HTN and immunoendocrine regulation of BP. Existing literature reveals heightened sympathetic nerve activity (SNA) in white coat and borderline hypertensive subjects [116, 117], and the magnitude of the elevation of SNA is related to the magnitude of hypertension [118, 119]. Like humans, SHR shows reduced cardiac parasympathetic nerve activity, elevated SNA and increased NA release [120, 121]. Here, we found neuro-adrenergic overdrive-induced HTN in CST-KO mice. Augmented SNA in HTN is known to activate both

myeloid cells and T cells [11, 122], and primary HTN shows increased circulating concentration of proinflammatory cytokines such as TNFα and IL6 [123]. To our knowledge, the present study is the 1st to demonstrate increased infiltration of macrophages in the adrenal medulla concomitant with increased secretion of CAs and the consequent development of HTN in CST-KO mice, which were normalized after CST supplementation. These findings imply that CST regulates BP through a novel immunoendocrine regulation of CA secretion.

Acknowledgments:

Supported by grants from the Veterans Affairs (I01 BX003934 to SKM; BX001963 to HHP) and the National Institutes of Health (AI141630 to P.G, GM138385 to D.S and HL091071, HL066941, AG053568, AG052914, AG052722 to HHP).

Author contributions:

W.Y., designed and generated CDN liposome, bone marrow transplantation and FACS analyses data. Provided inputs and edited the MS.

K.T., designed and generated qPCR, plasma cytokine, CgA and CST in tissue and plasma, and catecholamines in tissue and plasma data. Provided inputs and edited the MS.

E.A., designed and generated western blot data. Edited the MS.

J.M.S., designed and generated ischemia reperfusion and ischemic pre-conditioning data as well as made statistical analyses of the data.

T.P. and G.B., designed and generated glucose and fatty acid uptake and oxidation data.

M.A.L., generated blood pressure data. Edited the MS.

S.M., generated qPCR data and edited the MS.

S.D., Intellectual input in the analysis of the CST-KO immunophenotype (gene expression and reactome pathway).

H.H.P., supervised ischemia reperfusion and ischemic pre-conditioning studies and provided financial support for those studies.

N.J.G.W., designed and generated microarray data and edited the MS

D.S., Analyzed and interpreted the microarray dataset, generated heat map.

P.G., Extensively edited the MS and Figures, interpreted transcriptomic dataset, made Figures and provided crucial inputs on the overall organization of the MS and Figures.

S.K.M., conceived the idea, generated TEM data, supervised >90% of the studies, analyzed the data and made the graphics with extensive inputs from P.G., wrote the MS with extensive inputs from P.G. and provided financial support (>95%).

636

637

638 **Disclosures:**

639 None

640

642 **Figure legends**

643 **Fig. 1. CST-KO mice have enlarged hearts.**

644 **(A) Schematic diagram showing the cloning strategy for generating CST-KO mice. (B)**
645 **Western blot showing the presence of CgA in the left ventricle of WT and CST-KO mice.**
646 Mouse monoclonal antibody 5A8 detects full-length CgA (~70 kDa). While WT mice showed a
647 band of ~70 kDa, CST-KO mice showed a proteoglycan form of CgA. **(C) Western blot showing**
648 **the presence of CgA and CST.** A rabbit polyclonal antibody against the C-terminal domain of
649 CST (P_{368}-R_{373}) detects CST as well as CgA up to $CgA_{1\text{-}373}$. In the WT mice, this antibody detected
650 a proteolytically processed CgA (~45 kDa spanning $CgA_{1\text{-}373}$) and detected no band in CST-KO
651 mice, confirming deletion of CST domain. **(D). Graph display adrenal CgA.** A commercial mouse
652 EIA kit (CUSABIO Technology LLC, Houston, TX) was used to determine adrenal CgA content in
653 WT and CST-KO mice. **(E) Graph display plasma CST (n=6).** A commercial mouse EIA kit
654 (RayBiotech Life, GA) was used to determine plasma CST level in WT and CST-KO mice. **(F)**
655 **Size of wet heart.** Hearts were dissected out from WT and CST-KO mice and placed on top of a
656 piece of paper. Photographs show bigger heart in CST-KO mice compared to WT mice. **(G)**
657 **Weight of wet heart (n=16).** CST-KO wet heart was 27.5% heavier than WT heart when
658 normalized to body weight. **(H) Systolic BP (n=12).** SBP in WT and CST-KO mice. A tail-cuff
659 method (MRBP, IITC Inc. Life Science, CA) was used to determine SBP. DTA, diphtheria toxin;
660 FRT, *Flp* recognition target. ***p<0.001.

661

662 **Fig. 2. CST-KO mice are hypertensive, display systemic and cardiac inflammation; all**
663 **phenotypes are reversed by exogenous CST (2 µg/g body weight for 3 weeks).**

664 **(A) Schematic diagram** showing the interventional studies done on mice. **(B) Plasma CST** after
665 saline or 24 hr of CST treatment (n=6). The EIA kit used in Fig 1D above was used to measure
666 plasma CST **(C) Plasma cytokines** in saline or CST treated WT and CST-KO mice (n=8). U-
667 PLEX mouse cytokine assay kit (Meso Scale Diagnostics, Rockville, MD) was used to determine
668 plasma cytokine levels. **(D) RT-qPCR data** showing steady-state mRNA levels of anti-
669 inflammatory cytokines in left ventricle (n=8). Note increased expression of anti-inflammatory
670 genes in CST-KO mice after 3 weeks of treatment with CST. In WT mice, CST treatment caused
671 increased expression of *IL10*, *Mrc1* and *Arg1 genes*. **(E) RT-qPCR data** showing steady-state
672 mRNA levels of proinflammatory cytokines in left ventricle (n=8). Note increased mRNA levels of
673 proinflammatory genes in saline-treated CST-KO mice. Treatments of CST-KO mice with CST
674 caused significant decrease in mRNA levels. Ns, not significant; *p<0.05; **p<0.01; ***p<0.001.

675

Fig. 3. Macrophages are key mediators of the proinflammatory cardiovascular phenotypes in the CST-KO mice.

(A) Schematic diagram showing the interventional studies done on mice. (B) Systolic blood pressure (SBP) after saline or 3 weeks of CST treatment. A tail-cuff method (MRBP, IITC Inc. Life Science, CA) was used to determine SBP in saline or CST-treated conscious mice. **(C, F&G) Ultrastructural demonstration** of macrophages in WT and CST-KO heart (n=4). **(C) Saline-treated** WT and CST-KO heart. Note the presence of none or a single resident macrophage **in** WT heart and infiltrated macrophages in CST-KO heart. **(D) FACS data** showing macrophage population in CST-KO heart after treatment with saline or CST (n=3). **(E) Bar graph** showing CD45+ leukocytes in CST-KO mice in presence or absence of CST. **(F) CST-treated WT and CST-KO heart**. Note the presence of only resident macrophages. **(G) Chlodronate (CDN)-treated** WT and CST-KO heart. Note complete absence of macrophages. **(H) SBP** after depletion of macrophages by CDN (n=8). Note significant decrease (by 36 mmHg) in BP after CDN. **(I) SBP** after bone marrow transplantation (BMT) into irradiated mice (n=8). Note increased BP in WT mice after receiving CST-KO-BMT and decreased BP in CST-KO mice after receiving WT-BMT. **(J) Plasma CST** in BMT mice (n=6). Note macrophage-derived CST in CST-KO mice that received WT-BMT. IFM, intermyofibrillar mitochondria; Mϕ, macrophage; ns, not significant; SSM, sub-sarcolemmal mitochondria; *p<0.05; **p<0.01; ***p<0.001.

Fig. 4. Analysis of cardiac transcripts in CST-KO mice reveal defects in the core myocardial functions.

(A) Gene array data showing differential expression of genes (log2) in WT and CST-KO mice (n=5). **(B) RT-qPCR data** validating gene array data as well as expression after CST supplementation (n=6). (**C**) **Expression of sarcomere genes** in WT and CST-KO mice after treatment with saline or CST (n=6)**. (F) Expression of mitochondrial genes** in WT and CST-KO mice after treatment with saline or CST (n=6). Ns, not significant; *p<0.05; **p<0.01; ***p<0.001.

Fig. 5. CST-KO mice display an altered cardiometabolic phenotype, insulin resistance

(A) 2-deoxy-glucose (2DG) uptake and gluclose-6-phosphate (G6P) utilization 90 min after 2DG injection (n=6). **(B) Relative expression of genes involved in glucose metabolism (n=6). (C) Fatty acid (palmitic acid) uptake and oxidation (acid soluble metabolite: ASM)** 90 min after injection of palmitic acid (n=6). (**D**) **Relative expression of genes involved in fat metabolism and fat metabolites (n=6). (E) Cardiac glycogen** level in WT and CST-KO mice after treatment with saline or CST (n=6). **(F) Morphometric analyses** of glycogen granules. **(G)**

Ultrastructural demonstration of glycogen granules (GG) in ventricle of WT and CST-KO mice after treatment with saline or CST. **(H) Immunoblot data (n=4).** Representative western blots (12 hr fasting; n=4) from left ventricle of 4 mice in each group. **(I&J)** Densitometric values: **(I)** AKT and **(J)** GSK-3β. Ns, not significant; *p<0.05; **p<0.01; ***p<0.001.

Fig. 6. CST-KO mice display altered mitochondrial morphology

Transmission Electron Microscopic (TEM) images showing mitochondria and cristae (n=4). (A-D) Low magnification micrographs showing sub-sarcolemmal mitochondria (SSM). Note the presence of mitophagy (Mp) in saline-treated CST-KO mice **(C),** which was abolished after treatment with CST **(D). (E-H) High magnification micrographs** showing SSM. Note broken and smaller cristae in saline-treated CST-KO mice **(G),** which were restored after treatment with CST **(H). (I-L) Low magnification micrographs** showing inter- or intramyofibrillar mitochondria (IFM). Note the presence of lipid droplets (LD) juxtaposed to IFM in saline-treated CST-KO mice **(L),** which were dramatically reduced after treatment with CST **(L). (M-P) High magnification micrographs** showing IFM. Note broken and smaller cristae in saline-treated CST-KO mice **(O),** which were restored after treatment with CST **(P). (Q) High magnification IFM** showing LD. **(R) High magnification SSM** showing mitophagy (Mp). **(S) Morphometric data** showing decreased cristae surface area in saline-treated CST-KO mice, which were restored in CST-treated CST-KO mice. Ns, not significant; *p<0.05.

Fig. 7. CST-KO mice display inflamed adrenal medulla and altered catecholamine secretion

TEM micrographs of the adrenal medulla (n=4). (A) Low magnification micrographs showing resident macrophage in WT mice and resident plus infiltrated macrophages in CST-KO mice in presence or absence of CST or CDN. Note close association of macrophage with the axon terminal (AT) of the splanchnic nerve in CST-KO mice, indicating crosstalk between macrophages and synaptic vesicles. (**B) Adrenal catecholamines** (n=12). CST-KO mice store more norepinephrine (NE) than WT mice. **(C) Plasma catecholamines** (n=12). Note increased plasma DA, NE and epinephrine (EPI) levels in CST-KO mice, which were significantly reduced by supplementation with CST. **(D)** High magnification micrographs showing chromaffin granules (CG) in the adrenal medulla. Note docked CG in CST-KO mice. (**E**) High magnification micrographs showing splanchnico-adrenomedullary synapse with clear acetylcholine vesicles (AChV) and dense core peptidergic vesicles (PdV). CC, chromaffin cell; Mϕ, macrophage; ns, not significant; *p<0.05; **p<0.01; ***p<0.001

744 **Fig. 8. Summary or findings and working model.**

745 Schematic showing the major conclusions from the current work and its relevance to human
746 cardiovascular health and HTN. Based on our findings in CST-KO mice, and prior work
747 demonstrating the association of SNPs in CST with HTN and CVD, we propose a model wherein
748 CST maintains cardiac homeostasis and prevents HTN *via* two major mechanisms-- First, it exerts
749 an anti-inflammatory action *via* its effect on macrophage processes and polarization. Second, it
750 exerts a negative feedback loop on CA secretion from chromaffin cells [13, 124, 125]. In the absence
751 of CST, serum CA (e.g., NE) is elevated and macrophages become reactive in phenotype. While
752 the former results in HTN, the latter causes inflammation in the adrenals and heart. Macrophage
753 infiltration in the heart and local secretion of cytokines by activated macrophages result in altered
754 myocardial ultrastructure, bioenergetics, cardiometabolic shift, insulin resistance, and core
755 myocardial functions, e.g., ischemic preconditioning related protection. In doing so, CST acts as
756 a central mediator of cardiovascular homeostasis *via* a complex immunoendocrine axis.
757

Supplementary Figure Legends

Fig. S1. Screening of CST-KO mice by PCR. Primer set 1 was designed flanking the CST domain. CST-KO mice showed a PCR product of 162 bp compared to 225 bp in WT mice. Reverse primer 2 was designed from the CST domain. Therefore, there will be no PCR product in CST-KO mice when primer set 2 was used. The WT mice showed a product of 180 bp.

Fig. S2. Depletion of macrophages by clodronate liposomes. The cardiac macrophage population was evaluated by FACS analysis after treatment of clodronate liposomes (n=4 mice per group). Cardiac macrophage: $CD45^{+}CD11b^{+}F4/80^{+}$.

Fig. S3. IPC-induced cardioprotection against I/R injury. Hearts were excised and perfused on a Langendorff apparatus for I/R and IPC studies. **LVDP.** Changes in LVDP are shown in **A** and **B**. We found a significant effect of time (p<0.001), and time * strain * protocol (p=0.042), with no significant effect for time * strain, and time * protocol. **LVEDP.** Changes in LVEDP are shown in **C** and **D**. There was a significant effect of time (p<0.001), and time * strain * protocol (p<0.001), with no significant effect for time * strain, and time * protocol. **dP/dt_{max}:** Changes in dP/dt_{max} are shown in **E** and **F**. There was a significant effect of time (p<0.001), with no significant effect for time * strain, and time * protocol, or time * strain * protocol. **dP/dt_{min}**. Changes in dP/dt_{min} are shown in **G** and **H**. There was a significant effect of time (p<0.001), and time * protocol (p=0.004), with no significant effect for time * strain, and time * strain * protocol.

References

1. Bromfield S, Muntner P. High blood pressure: The leading global burden of disease risk factor and the need for worldwide prevention programs. *Curr Hypertens Rep*. 2013;15:134-136
2. Forouzanfar MH, Liu P, Roth GA, Ng M, Biryukov S, Marczak L, Alexander L, Estep K, Hassen Abate K, Akinyemiju TF, Ali R, Alvis-Guzman N, Azzopardi P, Banerjee A, Barnighausen T, Basu A, Bekele T, Bennett DA, Biadgilign S, Catala-Lopez F, Feigin VL, Fernandes JC, Fischer F, Gebru AA, Gona P, Gupta R, Hankey GJ, Jonas JB, Judd SE, Khang YH, Khosravi A, Kim YJ, Kimokoti RW, Kokubo Y, Kolte D, Lopez A, Lotufo PA, Malekzadeh R, Melaku YA, Mensah GA, Misganaw A, Mokdad AH, Moran AE, Nawaz H, Neal B, Ngalesoni FN, Ohkubo T, Pourmalek F, Rafay A, Rai RK, Rojas-Rueda D, Sampson UK, Santos IS, Sawhney M, Schutte AE, Sepanlou SG, Shifa GT, Shiue I, Tedla BA, Thrift AG, Tonelli M, Truelsen T, Tsilimparis N, Ukwaja KN, Uthman OA, Vasankari T, Venketasubramanian N, Vlassov VV, Vos T, Westerman R, Yan LL, Yano Y, Yonemoto N, Zaki ME, Murray CJ. Global burden of hypertension and systolic blood pressure of at least 110 to 115 mm hg, 1990-2015. *JAMA*. 2017;317:165-182
3. Goldstein DS. Plasma catecholamines and essential hypertension. An analytical review. *Hypertension*. 1983;5:86-99
4. Floras JS. Epinephrine and the genesis of hypertension. *Hypertension*. 1992;19:1-18
5. Mathar I, Vennekens R, Meissner M, Kees F, Van der Mieren G, Camacho Londono JE, Uhl S, Voets T, Hummel B, van den Bergh A, Herijgers P, Nilius B, Flockerzi V, Schweda F, Freichel M. Increased catecholamine secretion contributes to hypertension in trpm4-deficient mice. *J Clin Invest*. 2010;120:3267-3279
6. Currie G, Freel EM, Perry CG, Dominiczak AF. Disorders of blood pressure regulation-role of catecholamine biosynthesis, release, and metabolism. *Curr Hypertens Rep*. 2012;14:38-45
7. Fisher JP, Paton JF. The sympathetic nervous system and blood pressure in humans: Implications for hypertension. *J Hum Hypertens*. 2012;26:463-475
8. Dzielak DJ. Immune mechanisms in experimental and essential hypertension. *Am J Physiol*. 1991;260:R459-467
9. Coffman TM. Under pressure: The search for the essential mechanisms of hypertension. *Nat Med*. 2011;17:1402-1409
10. Byrne CJ, Khurana S, Kumar A, Tai TC. Inflammatory signaling in hypertension: Regulation of adrenal catecholamine biosynthesis. *Front Endocrinol (Lausanne)*. 2018;9:343
11. Norlander AE, Madhur MS, Harrison DG. The immunology of hypertension. *J Exp Med*. 2018;215:21-33
12. Sesso HD, Buring JE, Rifai N, Blake GJ, Gaziano JM, Ridker PM. C-reactive protein and the risk of developing hypertension. *JAMA*. 2003;290:2945-2951
13. Mahata SK, O'Connor DT, Mahata M, Yoo SH, Taupenot L, Wu H, Gill BM, Parmer RJ. Novel autocrine feedback control of catecholamine release. A discrete chromogranin a fragment is a noncompetitive nicotinic cholinergic antagonist. *J Clin Invest*. 1997;100:1623-1633
14. Winkler H, Fischer-Colbrie R. The chromogranins a and b: The first 25 years and future perspectives. *Neuroscience*. 1992;49:497-528
15. Montero-Hadjadje M, Vaingankar S, Elias S, Tostivint H, Mahata SK, Anouar Y. Chromogranins a and b and secretogranin ii: Evolutionary and functional aspects. *Acta Physiol (Oxf)*. 2008;192:309-324

16. Bartolomucci A, Possenti R, Mahata SK, Fischer-Colbrie R, Loh YP, Salton SR. The extended granin family: Structure, function, and biomedical implications. *Endocr Rev*. 2011;32:755-797
17. Chen Y, Rao F, Rodriguez-Flores JL, Mahapatra NR, Mahata M, Wen G, Salem RM, Shih PA, Das M, Schork NJ, Ziegler MG, Hamilton BA, Mahata SK, O'Connor DT. Common genetic variants in the chromogranin a promoter alter autonomic activity and blood pressure. *Kidney Int*. 2008;74:115-125
18. O'Connor DT, Zhu G, Rao F, Taupenot L, Fung MM, Das M, Mahata SK, Mahata M, Wang L, Zhang K, Greenwood TA, Shih PA, Cockburn MG, Ziegler MG, Stridsberg M, Martin NG, Whitfield JB. Heritability and genome-wide linkage in us and australian twins identify novel genomic regions controlling chromogranin a: Implications for secretion and blood pressure. *Circulation*. 2008;118:247-257
19. O'Connor DT, Takiyyuddin MA, Printz MP, Dinh TQ, Barbosa JA, Rozansky DJ, Mahata SK, Wu H, Kennedy BP, Ziegler MG, Wright FA, Schlager G, Parmer RJ. Catecholamine storage vesicle protein expression in genetic hypertension. *Blood Press*. 1999;8:285-295
20. O'Connor DT, Kailasam MT, Kennedy BP, Ziegler MG, Yanaihara N, Parmer RJ. Early decline in the catecholamine release-inhibitory peptide catestatin in humans at genetic risk of hypertension. *J Hypertens*. 2002;20:1335-1345
21. Wen G, Mahata SK, Cadman P, Mahata M, Ghosh S, Mahapatra NR, Rao F, Stridsberg M, Smith DW, Mahboubi P, Schork NJ, O'Connor DT, Hamilton BA. Both rare and common polymorphisms contribute functional variation at chga, a regulator of catecholamine physiology. *Am J Hum Genet*. 2004;74:197-207
22. Rao F, Wen G, Gayen JR, Das M, Vaingankar SM, Rana BK, Mahata M, Kennedy BP, Salem RM, Stridsberg M, Abel K, Smith DW, Eskin E, Schork NJ, Hamilton BA, Ziegler MG, Mahata SK, O'Connor DT. Catecholamine release-inhibitory peptide catestatin (chromogranin a(352-372)): Naturally occurring amino acid variant gly364ser causes profound changes in human autonomic activity and alters risk for hypertension. *Circulation*. 2007;115:2271-2281
23. Biswas N, Vaingankar SM, Mahata M, Das M, Gayen JR, Taupenot L, Torpey JW, O'Connor DT, Mahata SK. Proteolytic cleavage of human chromogranin a containing naturally occurring catestatin variants: Differential processing at catestatin region by plasmin. *Endocrinology*. 2008;149:749-757
24. Angelone T, Quintieri AM, Brar BK, Limchaiyawat PT, Tota B, Mahata SK, Cerra MC. The antihypertensive chromogranin a peptide catestatin acts as a novel endocrine/paracrine modulator of cardiac inotropism and lusitropism. *Endocrinology*. 2008;149:4780-4793
25. Biswas N, Rodriguez-Flores JL, Courel M, Gayen JR, Vaingankar SM, Mahata M, Torpey JW, Taupenot L, O'Connor DT, Mahata SK. Cathepsin l co-localizes with chromogranin a in chromaffin vesicles to generate active peptides. *Endocrinology*. 2009;150:3547-3557
26. Sahu BS, Obbineni JM, Sahu G, Allu PK, Subramanian L, Sonawane PJ, Singh PK, Sasi BK, Senapati S, Maji SK, Bera AK, Gomathi BS, Mullasari AS, Mahapatra NR. Functional genetic variants of the catecholamine-release-inhibitory peptide catestatin in an indian population: Allele-specific effects on metabolic traits. *J Biol Chem*. 2012;287:43840-43852
27. Choi Y, Miura M, Nakata Y, Sugasawa T, Nissato S, Otsuki T, Sugawara J, Iemitsu M, Kawakami Y, Shimano H, Iijima Y, Tanaka K, Kuno S, Allu PK, Mahapatra NR, Maeda S, Takekoshi K. A common genetic variant of the chromogranin a-derived peptide catestatin is associated with atherogenesis and hypertension in a japanese population. *Endocr J*. 2015;62:797-804
28. Kiranmayi M, Chirasani VR, Allu PK, Subramanian L, Martelli EE, Sahu BS, Vishnuprabu D, Kumaragurubaran R, Sharma S, Bodhini D, Dixit M, Munirajan AK, Khullar M, Radha V, Mohan V, Mullasari AS, Naga Prasad SV, Senapati S, Mahapatra NR. Catestatin

gly364ser variant alters systemic blood pressure and the risk for hypertension in human populations via endothelial nitric oxide pathway. *Hypertension*. 2016

29. Ottesen AH, Carlson CR, Louch WE, Dahl MB, Sandbu RA, Johansen RF, Jarstadmarken H, Bjoras M, Hoiseth AD, Brynildsen J, Sjaastad I, Stridsberg M, Omland T, Christensen G, Rosjo H. Glycosylated chromogranin a in heart failure: Implications for processing and cardiomyocyte calcium homeostasis. *Circ Heart Fail*. 2017;10
30. Mahapatra NR, O'Connor DT, Vaingankar SM, Hikim AP, Mahata M, Ray S, Staite E, Wu H, Gu Y, Dalton N, Kennedy BP, Ziegler MG, Ross J, Mahata SK. Hypertension from targeted ablation of chromogranin a can be rescued by the human ortholog. *J Clin Invest*. 2005;115:1942-1952
31. Bandyopadhyay GK, Vu CU, Gentile S, Lee H, Biswas N, Chi NW, O'Connor DT, Mahata SK. Catestatin (chromogranin a(352-372)) and novel effects on mobilization of fat from adipose tissue through regulation of adrenergic and leptin signaling. *J Biol Chem*. 2012;287:23141-23151
32. Ratti S, Curnis F, Longhi R, Colombo B, Gasparri A, Magni F, Manera E, Metz-Boutigue MH, Corti A. Structure-activity relationships of chromogranin a in cell adhesion. Identification of an adhesion site for fibroblasts and smooth muscle cells [in process citation]. *J Biol Chem*. 2000;275:29257-29263
33. Bianco M, Gasparri AM, Colombo B, Curnis F, Girlanda S, Ponzoni M, Bertilaccio MT, Calcinotto A, Sacchi A, Ferrero E, Ferrarini M, Chesi M, Bergsagel PL, Bellone M, Tonon G, Ciceri F, Marcatti M, Caligaris-Cappio F, Corti A. Chromogranin a is preferentially cleaved into proangiogenic peptides in the bone marrow of multiple myeloma patients. *Cancer Res*. 2016;76:1781-1791
34. Hulsmans M, Sager HB, Roh JD, Valero-Munoz M, Houstis NE, Iwamoto Y, Sun Y, Wilson RM, Wojtkiewicz G, Tricot B, Osborne MT, Hung J, Vinegoni C, Naxerova K, Sosnovik DE, Zile MR, Bradshaw AD, Liao R, Tawakol A, Weissleder R, Rosenzweig A, Swirski FK, Sam F, Nahrendorf M. Cardiac macrophages promote diastolic dysfunction. *J Exp Med*. 2018;215:423-440
35. Pasqua T, Mahata S, Bandyopadhyay GK, Biswas A, Perkins GA, Sinha-Hikim AP, Goldstein DS, Eiden LE, Mahata SK. Impact of chromogranin a deficiency on catecholamine storage, catecholamine granule morphology and chromaffin cell energy metabolism in vivo. *Cell Tissue Res*. 2016;363:693-712
36. Hsiao A, Worrall DS, Olefsky JM, Subramaniam S. Variance-modeled posterior inference of microarray data: Detecting gene-expression changes in 3t3-l1 adipocytes. *Bioinformatics*. 2004;20:3108-3127
37. Bligh EG, Dyer WJ. A rapid method of total lipid extraction and purification. *Can J Biochem Physiol*. 1959;37:911-917
38. Folch J, Lees M, Sloane Stanley GH. A simple method for the isolation and purification of total lipides from animal tissues. *J Biol Chem*. 1957;226:497-509
39. Tang K, Pasqua T, Biswas A, Mahata S, Tang J, Tang A, Bandyopadhyay GK, Sinha-Hikim AP, Chi NW, Webster NJ, Corti A, Mahata SK. Muscle injury, impaired muscle function and insulin resistance in chromogranin a-knockout mice. *J Endocrinol*. 2017;232:137-153
40. Carroll NV, Longley RW, Roe JH. The determination of glycogen in liver and muscle by use of anthrone reagent. *J Biol Chem*. 1956;220:583-593
41. Headrick JP, Willems L, Ashton KJ, Holmgren K, Peart J, Matherne GP. Ischaemic tolerance in aged mouse myocardium: The role of adenosine and effects of a1 adenosine receptor overexpression. *J Physiol*. 2003;549:823-833
42. Ying W, Mahata S, Bandyopadhyay GK, Zhou Z, Wollam J, Vu J, Mayoral R, Chi NW, Webster NJG, Corti A, Mahata SK. Catestatin inhibits obesity-induced macrophage

infiltration and inflammation in the liver and suppresses hepatic glucose production, leading to improved insulin sensitivity. *Diabetes*. 2018;67:841-848

43. Kojima M, Ozawa N, Mori Y, Takahashi Y, Watanabe-Kominato K, Shirai R, Watanabe R, Sato K, Matsuyama TA, Ishibashi-Ueda H, Koba S, Kobayashi Y, Hirano T, Watanabe T. Catestatin prevents macrophage-driven atherosclerosis but not arterial injury-induced neointimal hyperplasia. *Thromb Haemost*. 2018;118:182-194
44. Chen H, Liu D, Ge L, Wang T, Ma Z, Han Y, Duan Y, Xu X, Liu W, Yuan J, Liu J, Li R, Du R. Catestatin prevents endothelial inflammation and promotes thrombus resolution in acute pulmonary embolism in mice. *Biosci Rep*. 2019;39
45. Zivkovic PM, Matetic A, Tadin Hadjina I, Rusic D, Vilovic M, Supe-Domic D, Borovac JA, Mudnic I, Tonkic A, Bozic J. Serum catestatin levels and arterial stiffness parameters are increased in patients with inflammatory bowel disease. *J Clin Med*. 2020;9
46. Avolio E, Mahata SK, Mantuano E, Mele M, Alo R, Facciolo RM, Talani G, Canonaco M. Antihypertensive and neuroprotective effects of catestatin in spontaneously hypertensive rats: Interaction with gabaergic transmission in amygdala and brainstem. *Neuroscience*. 2014;270:48-57
47. Granger JP. An emerging role for inflammatory cytokines in hypertension. *Am J Physiol Heart Circ Physiol*. 2006;290:H923-924
48. Lee DL, Sturgis LC, Labazi H, Osborne JB, Jr., Fleming C, Pollock JS, Manhiani M, Imig JD, Brands MW. Angiotensin ii hypertension is attenuated in interleukin-6 knockout mice. *Am J Physiol Heart Circ Physiol*. 2006;290:H935-940
49. Brands MW, Banes-Berceli AK, Inscho EW, Al-Azawi H, Allen AJ, Labazi H. Interleukin 6 knockout prevents angiotensin ii hypertension: Role of renal vasoconstriction and janus kinase 2/signal transducer and activator of transcription 3 activation. *Hypertension*. 2010;56:879-884
50. Lima VV, Zemse SM, Chiao CW, Bomfim GF, Tostes RC, Clinton Webb R, Giachini FR. Interleukin-10 limits increased blood pressure and vascular rhoa/rho-kinase signaling in angiotensin ii-infused mice. *Life Sci*. 2016;145:137-143
51. Ishimitsu T, Uehara Y, Numabe A, Tsukada H, Ogawa Y, Yagi S. Antihypertensive effect of interleukin-2 in salt-sensitive dahl rats. *Hypertension*. 1994;23:68-73
52. Tuttle RS, Boppana DP. Antihypertensive effect of interleukin-2. *Hypertension*. 1990;15:89-94
53. Tinsley JH, South S, Chiasson VL, Mitchell BM. Interleukin-10 reduces inflammation, endothelial dysfunction, and blood pressure in hypertensive pregnant rats. *Am J Physiol Regul Integr Comp Physiol*. 2010;298:R713-719
54. Viel EC, Lemarie CA, Benkirane K, Paradis P, Schiffrin EL. Immune regulation and vascular inflammation in genetic hypertension. *Am J Physiol Heart Circ Physiol*. 2010;298:H938-944
55. Ritterhoff J, Tian R. Metabolism in cardiomyopathy: Every substrate matters. *Cardiovasc Res*. 2017;113:411-421
56. Lopaschuk GD, Belke DD, Gamble J, Itoi T, Schonekess BO. Regulation of fatty acid oxidation in the mammalian heart in health and disease. *Biochim Biophys Acta*. 1994;1213:263-276
57. Stanley WC, Lopaschuk GD, Hall JL, McCormack JG. Regulation of myocardial carbohydrate metabolism under normal and ischaemic conditions. Potential for pharmacological interventions. *Cardiovasc Res*. 1997;33:243-257
58. Mishra PK, Ying W, Nandi SS, Bandyopadhyay GK, Patel KK, Mahata SK. Diabetic cardiomyopathy: An immunometabolic perspective. *Front Endocrinol (Lausanne)*. 2017;8:72
59. Sokolowska E, Blachnio-Zabielska A. The role of ceramides in insulin resistance. *Front Endocrinol (Lausanne)*. 2019;10:577

60. Dasgupta A, Bandyopadhyay GK, Ray I, Bandyopadhyay K, Chowdhury N, De RK, Mahata SK. Catestatin improves insulin sensitivity by attenuating endoplasmic reticulum stress: In vivo and in silico validation. *Comput Struct Biotechnol J*. 2020;18:464-481
61. Mehta MM, Weinberg SE, Chandel NS. Mitochondrial control of immunity: Beyond atp. *Nat Rev Immunol*. 2017;17:608-620
62. Touyz RM. Reactive oxygen species, vascular oxidative stress, and redox signaling in hypertension: What is the clinical significance? *Hypertension*. 2004;44:248-252
63. Cogliati S, Frezza C, Soriano ME, Varanita T, Quintana-Cabrera R, Corrado M, Cipolat S, Costa V, Casarin A, Gomes LC, Perales-Clemente E, Salviati L, Fernandez-Silva P, Enriquez JA, Scorrano L. Mitochondrial cristae shape determines respiratory chain supercomplexes assembly and respiratory efficiency. *Cell*. 2013;155:160-171
64. Hollander JM, Thapa D, Shepherd DL. Physiological and structural differences in spatially distinct subpopulations of cardiac mitochondria: Influence of cardiac pathologies. *Am J Physiol Heart Circ Physiol*. 2014;307:H1-14
65. Crochemore C, Mekki M, Corbiere C, Karoui A, Noel R, Vendeville C, Vaugeois JM, Monteil C. Subsarcolemmal and interfibrillar mitochondria display distinct superoxide production profiles. *Free Radic Res*. 2015;49:331-337
66. How OJ, Aasum E, Severson DL, Chan WY, Essop MF, Larsen TS. Increased myocardial oxygen consumption reduces cardiac efficiency in diabetic mice. *Diabetes*. 2006;55:466-473
67. Westermeier F, Navarro-Marquez M, Lopez-Crisosto C, Bravo-Sagua R, Quiroga C, Bustamante M, Verdejo HE, Zalaquett R, Ibacache M, Parra V, Castro PF, Rothermel BA, Hill JA, Lavandero S. Defective insulin signaling and mitochondrial dynamics in diabetic cardiomyopathy. *Biochim Biophys Acta*. 2015;1853:1113-1118
68. Gomes LC, Di Benedetto G, Scorrano L. During autophagy mitochondria elongate, are spared from degradation and sustain cell viability. *Nat Cell Biol*. 2011;13:589-598
69. Green DR, Galluzzi L, Kroemer G. Mitochondria and the autophagy-inflammation-cell death axis in organismal aging. *Science*. 2011;333:1109-1112
70. Delbridge LMD, Mellor KM, Taylor DJ, Gottlieb RA. Myocardial stress and autophagy: Mechanisms and potential therapies. *Nat Rev Cardiol*. 2017;14:412-425
71. Pende A, Musso NR, Vergassola C, Puppo F, Ioverno A, Criscuolo D, Indiveri F, Lotti G. Neuroendocrine effects of interferon alpha 2-a in healthy human subjects. *J Biol Regul Homeost Agents*. 1990;4:67-72
72. Corssmit EP, Heijligenberg R, Endert E, Ackermans MT, Sauerwein HP, Romijn JA. Endocrine and metabolic effects of interferon-alpha in humans. *J Clin Endocrinol Metab*. 1996;81:3265-3269
73. Kannan H, Tanaka Y, Kunitake T, Ueta Y, Hayashida Y, Yamashita H. Activation of sympathetic outflow by recombinant human interleukin-1 beta in conscious rats. *Am J Physiol*. 1996;270:R479-485
74. Rivier C, Vale W, Brown M. In the rat, interleukin-1 alpha and -beta stimulate adrenocorticotropin and catecholamine release. *Endocrinology*. 1989;125:3096-3102
75. Darling G, Goldstein DS, Stull R, Gorschboth CM, Norton JA. Tumor necrosis factor: Immune endocrine interaction. *Surgery*. 1989;106:1155-1160
76. De Laurentiis A, Pisera D, Caruso C, Candolfi M, Mohn C, Rettori V, Seilicovich A. Lipopolysaccharide- and tumor necrosis factor-alpha-induced changes in prolactin secretion and dopaminergic activity in the hypothalamic-pituitary axis. *Neuroimmunomodulation*. 2002;10:30-39
77. Epelman S, Lavine KJ, Beaudin AE, Sojka DK, Carrero JA, Calderon B, Brija T, Gautier EL, Ivanov S, Satpathy AT, Schilling JD, Schwendener R, Sergin I, Razani B, Forsberg EC, Yokoyama WM, Unanue ER, Colonna M, Randolph GJ, Mann DL. Embryonic and

adult-derived resident cardiac macrophages are maintained through distinct mechanisms at steady state and during inflammation. *Immunity*. 2014;40:91-104

78. Lavine KJ, Epelman S, Uchida K, Weber KJ, Nichols CG, Schilling JD, Ornitz DM, Randolph GJ, Mann DL. Distinct macrophage lineages contribute to disparate patterns of cardiac recovery and remodeling in the neonatal and adult heart. *Proc Natl Acad Sci U S A*. 2014;111:16029-16034
79. Leid J, Carrelha J, Boukarabila H, Epelman S, Jacobsen SE, Lavine KJ. Primitive embryonic macrophages are required for coronary development and maturation. *Circ Res*. 2016;118:1498-1511
80. Heo GS, Kopecky B, Sultan D, Ou M, Feng G, Bajpai G, Zhang X, Luehmann H, Detering L, Su Y, Leuschner F, Combadiere C, Kreisel D, Gropler RJ, Brody SL, Liu Y, Lavine KJ. Molecular imaging visualizes recruitment of inflammatory monocytes and macrophages to the injured heart. *Circ Res*. 2019;124:881-890
81. Bajpai G, Schneider C, Wong N, Bredemeyer A, Hulsmans M, Nahrendorf M, Epelman S, Kreisel D, Liu Y, Itoh A, Shankar TS, Selzman CH, Drakos SG, Lavine KJ. The human heart contains distinct macrophage subsets with divergent origins and functions. *Nat Med*. 2018;24:1234-1245
82. Bajpai G, Bredemeyer A, Li W, Zaitsev K, Koenig AL, Lokshina I, Mohan J, Ivey B, Hsiao HM, Weinheimer C, Kovacs A, Epelman S, Artyomov M, Kreisel D, Lavine KJ. Tissue resident ccr2- and ccr2+ cardiac macrophages differentially orchestrate monocyte recruitment and fate specification following myocardial injury. *Circ Res*. 2019;124:263-278
83. Heidt T, Courties G, Dutta P, Sager HB, Sebas M, Iwamoto Y, Sun Y, Da Silva N, Panizzi P, van der Laan AM, Swirski FK, Weissleder R, Nahrendorf M. Differential contribution of monocytes to heart macrophages in steady-state and after myocardial infarction. *Circ Res*. 2014;115:284-295
84. Mann DL. Innate immunity and the failing heart: The cytokine hypothesis revisited. *Circ Res*. 2015;116:1254-1268
85. Dick SA, Epelman S. Chronic heart failure and inflammation: What do we really know? *Circ Res*. 2016;119:159-176
86. Bergman MR, Kao RH, McCune SA, Holycross BJ. Myocardial tumor necrosis factor-alpha secretion in hypertensive and heart failure-prone rats. *Am J Physiol*. 1999;277:H543-550
87. Levine B, Kalman J, Mayer L, Fillit HM, Packer M. Elevated circulating levels of tumor necrosis factor in severe chronic heart failure. *N Engl J Med*. 1990;323:236-241
88. Kubota T, McTiernan CF, Frye CS, Slawson SE, Lemster BH, Koretsky AP, Demetris AJ, Feldman AM. Dilated cardiomyopathy in transgenic mice with cardiac-specific overexpression of tumor necrosis factor-alpha. *Circ Res*. 1997;81:627-635
89. Ashrafian H, Frenneaux MP, Opie LH. Metabolic mechanisms in heart failure. *Circulation*. 2007;116:434-448
90. Mootha VK, Arai AE, Balaban RS. Maximum oxidative phosphorylation capacity of the mammalian heart. *Am J Physiol*. 1997;272:H769-775
91. Balaban RS. Cardiac energy metabolism homeostasis: Role of cytosolic calcium. *J Mol Cell Cardiol*. 2002;34:1259-1271
92. Neubauer S. The failing heart--an engine out of fuel. *N Engl J Med*. 2007;356:1140-1151
93. Hall CJ, Sanderson LE, Crosier KE, Crosier PS. Mitochondrial metabolism, reactive oxygen species, and macrophage function-fishing for insights. *J Mol Med (Berl)*. 2014;92:1119-1128
94. Ingwall JS. Energy metabolism in heart failure and remodelling. *Cardiovasc Res*. 2009;81:412-419
95. Neely JR, Rovetto MJ, Oram JF. Myocardial utilization of carbohydrate and lipids. *Prog Cardiovasc Dis*. 1972;15:289-329

96. Taegtmeyer H, Golfman L, Sharma S, Razeghi P, van Arsdall M. Linking gene expression to function: Metabolic flexibility in the normal and diseased heart. *Ann N Y Acad Sci*. 2004;1015:202-213
97. Marelli-Berg FM, Aksentijevic D. Immunometabolic cross-talk in the inflamed heart. *Cell Stress*. 2019;3:240-266
98. Stanley WC, Recchia FA, Lopaschuk GD. Myocardial substrate metabolism in the normal and failing heart. *Physiol Rev*. 2005;85:1093-1129
99. Bertero E, Maack C. Metabolic remodelling in heart failure. *Nat Rev Cardiol*. 2018;15:457-470
100. Buchanan J, Mazumder PK, Hu P, Chakrabarti G, Roberts MW, Yun UJ, Cooksey RC, Litwin SE, Abel ED. Reduced cardiac efficiency and altered substrate metabolism precedes the onset of hyperglycemia and contractile dysfunction in two mouse models of insulin resistance and obesity. *Endocrinology*. 2005;146:5341-5349
101. Mazumder PK, O'Neill BT, Roberts MW, Buchanan J, Yun UJ, Cooksey RC, Boudina S, Abel ED. Impaired cardiac efficiency and increased fatty acid oxidation in insulin-resistant ob/ob mouse hearts. *Diabetes*. 2004;53:2366-2374
102. Wang P, Lloyd SG, Zeng H, Bonen A, Chatham JC. Impact of altered substrate utilization on cardiac function in isolated hearts from zucker diabetic fatty rats. *Am J Physiol Heart Circ Physiol*. 2005;288:H2102-2110
103. Lopaschuk GD, Folmes CD, Stanley WC. Cardiac energy metabolism in obesity. *Circ Res*. 2007;101:335-347
104. Fukushima A, Lopaschuk GD. Cardiac fatty acid oxidation in heart failure associated with obesity and diabetes. *Biochim Biophys Acta*. 2016;1861:1525-1534
105. Chess DJ, Stanley WC. Role of diet and fuel overabundance in the development and progression of heart failure. *Cardiovasc Res*. 2008;79:269-278
106. Rimbaud S, Ruiz M, Piquereau J, Mateo P, Fortin D, Veksler V, Garnier A, Ventura-Clapier R. Resveratrol improves survival, hemodynamics and energetics in a rat model of hypertension leading to heart failure. *PLoS One*. 2011;6:e26391
107. Lopaschuk GD, Ussher JR, Folmes CD, Jaswal JS, Stanley WC. Myocardial fatty acid metabolism in health and disease. *Physiol Rev*. 2010;90:207-258
108. Zlobine I, Gopal K, Ussher JR. Lipotoxicity in obesity and diabetes-related cardiac dysfunction. *Biochim Biophys Acta*. 2016;1861:1555-1568
109. Nakanishi T, Kato S. Impact of diabetes mellitus on myocardial lipid deposition: An autopsy study. *Pathol Res Pract*. 2014;210:1018-1025
110. D'Souza K, Nzirorera C, Kienesberger PC. Lipid metabolism and signaling in cardiac lipotoxicity. *Biochim Biophys Acta*. 2016;1861:1513-1524
111. Unger RH. Lipotoxic diseases. *Annu Rev Med*. 2002;53:319-336
112. Peterson LR, Herrero P, Schechtman KB, Racette SB, Waggoner AD, Kisrieva-Ware Z, Dence C, Klein S, Marsala J, Meyer T, Gropler RJ. Effect of obesity and insulin resistance on myocardial substrate metabolism and efficiency in young women. *Circulation*. 2004;109:2191-2196
113. Gray S, Kim JK. New insights into insulin resistance in the diabetic heart. *Trends in endocrinology and metabolism: TEM*. 2011;22:394-403
114. Rider OJ, Lewis AJ, Neubauer S. Structural and metabolic effects of obesity on the myocardium and the aorta. *Obes Facts*. 2014;7:329-338
115. Smith EL, Schuchman EH. The unexpected role of acid sphingomyelinase in cell death and the pathophysiology of common diseases. *FASEB J*. 2008;22:3419-3431
116. Anderson EA, Sinkey CA, Lawton WJ, Mark AL. Elevated sympathetic nerve activity in borderline hypertensive humans. Evidence from direct intraneural recordings. *Hypertension*. 1989;14:177-183

117. Smith PA, Graham LN, Mackintosh AF, Stoker JB, Mary DA. Relationship between central sympathetic activity and stages of human hypertension. *Am J Hypertens*. 2004;17:217-222
118. Grassi G, Cattaneo BM, Seravalle G, Lanfranchi A, Mancia G. Baroreflex control of sympathetic nerve activity in essential and secondary hypertension. *Hypertension*. 1998;31:68-72
119. Grassi G. Role of the sympathetic nervous system in human hypertension. *J Hypertens*. 1998;16:1979-1987
120. Judy WV, Farrell SK. Arterial baroreceptor reflex control of sympathetic nerve activity in the spontaneously hypertensive rat. *Hypertension*. 1979;1:605-614
121. Lundin S, Ricksten SE, Thoren P. Renal sympathetic activity in spontaneously hypertensive rats and normotensive controls, as studied by three different methods. *Acta Physiol Scand*. 1984;120:265-272
122. Elenkov IJ, Wilder RL, Chrousos GP, Vizi ES. The sympathetic nerve--an integrative interface between two supersystems: The brain and the immune system. *Pharmacol Rev*. 2000;52:595-638
123. Libby P, Ridker PM, Maseri A. Inflammation and atherosclerosis. *Circulation*. 2002;105:1135-1143
124. Mahata SK, Mahata M, Wakade AR, O'Connor DT. Primary structure and function of the catecholamine release inhibitory peptide catestatin (chromogranin a344-364): Identification of amino acid residues crucial for activity. *Mol Endocrinol*. 2000;14:1525-1535
125. Mahata SK, Mahapatra NR, Mahata M, Wang TC, Kennedy BP, Ziegler MG, O'Connor DT. Catecholamine secretory vesicle stimulus-transcription coupling in vivo. Demonstration by a novel transgenic promoter/photoprotein reporter and inhibition of secretion and transcription by the chromogranin a fragment catestatin. *J Biol Chem*. 2003;278:32058-32067

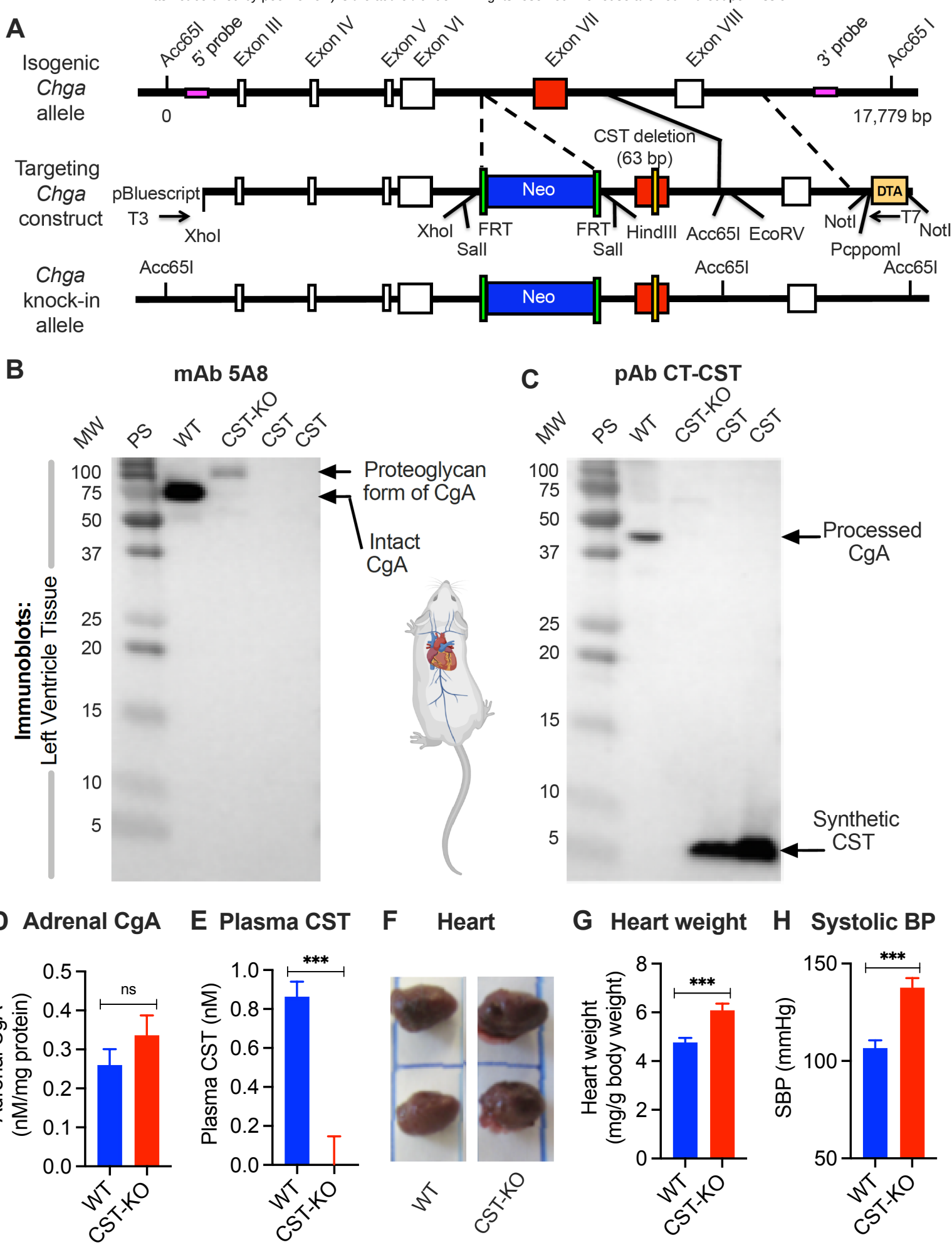
A
Isogenic Chga allele
Acc65I
5' probe
Exon III
Exon IV
Exon V
Exon VI
Exon VII
Exon VIII
3' probe
Acc65 I
0
17,779 bp
CST deletion (63 bp)
Targeting Chga construct
pBluescript
T3
XhoI
Neo
XhoI
FRT
SalI
FRT
SalI
HindIII
Acc65I
EcoRV
DTA
NotI
T7
NotI
PcppomI
Acc65I
Acc65I
Acc65I
Chga knock-in allele
Neo
B
mAb 5A8
MW
PS
WT
CST-KO
CST
CST
100
75
50
37
25
20
15
10
5
Proteoglycan form of CgA
Intact CgA
Immunoblots:
Left Ventricle Tissue
C
pAb CT-CST
MW
PS
WT
CST-KO
CST
CST
100
75
50
37
25
20
15
10
5
Processed CgA
Synthetic CST
D Adrenal CgA
Adrenal CgA (nM/mg protein)
0.5
0.4
0.3
0.2
0.1
0.0
ns
WT
CST-KO
E Plasma CST
Plasma CST (nM)
1.0
0.8
0.6
0.4
0.2
0.0
***
WT
CST-KO
F Heart
WT
CST-KO
G Heart weight
Heart weight (mg/g body weight)
8
6
4
2
0
***
WT
CST-KO
H Systolic BP
SBP (mmHg)
150
100
50
***
WT
CST-KO

Fig. 1

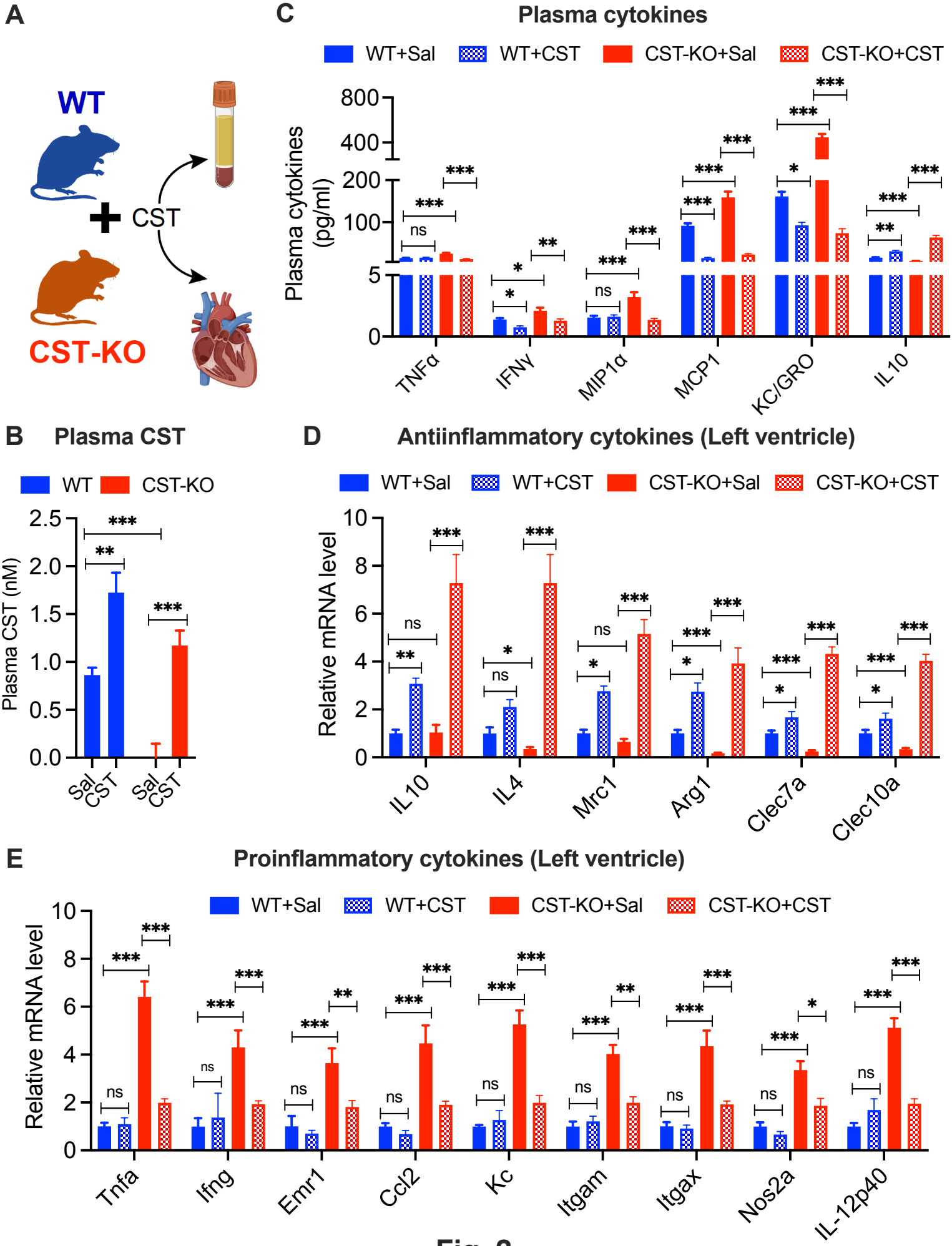

Fig. 2

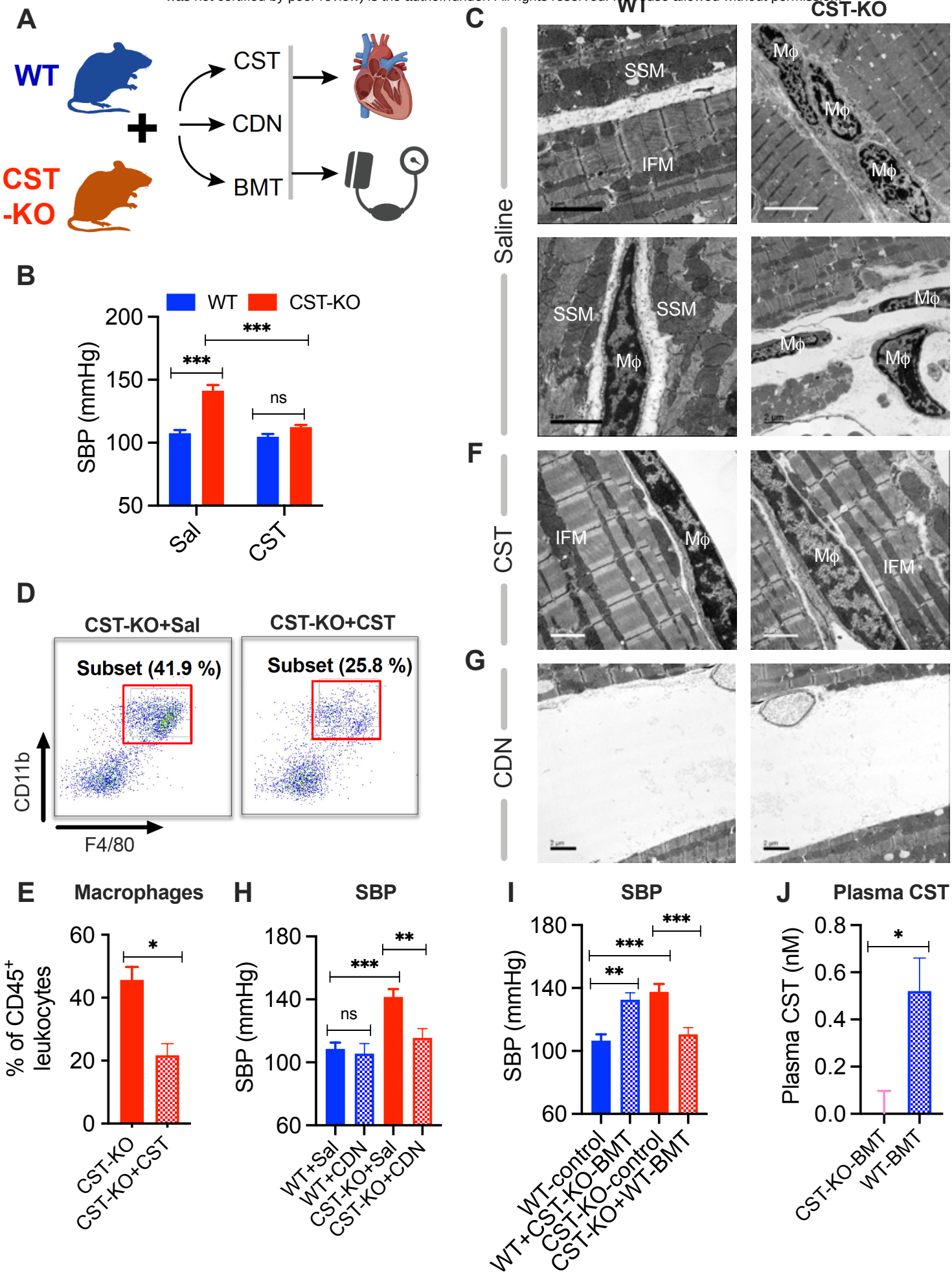

Fig. 3

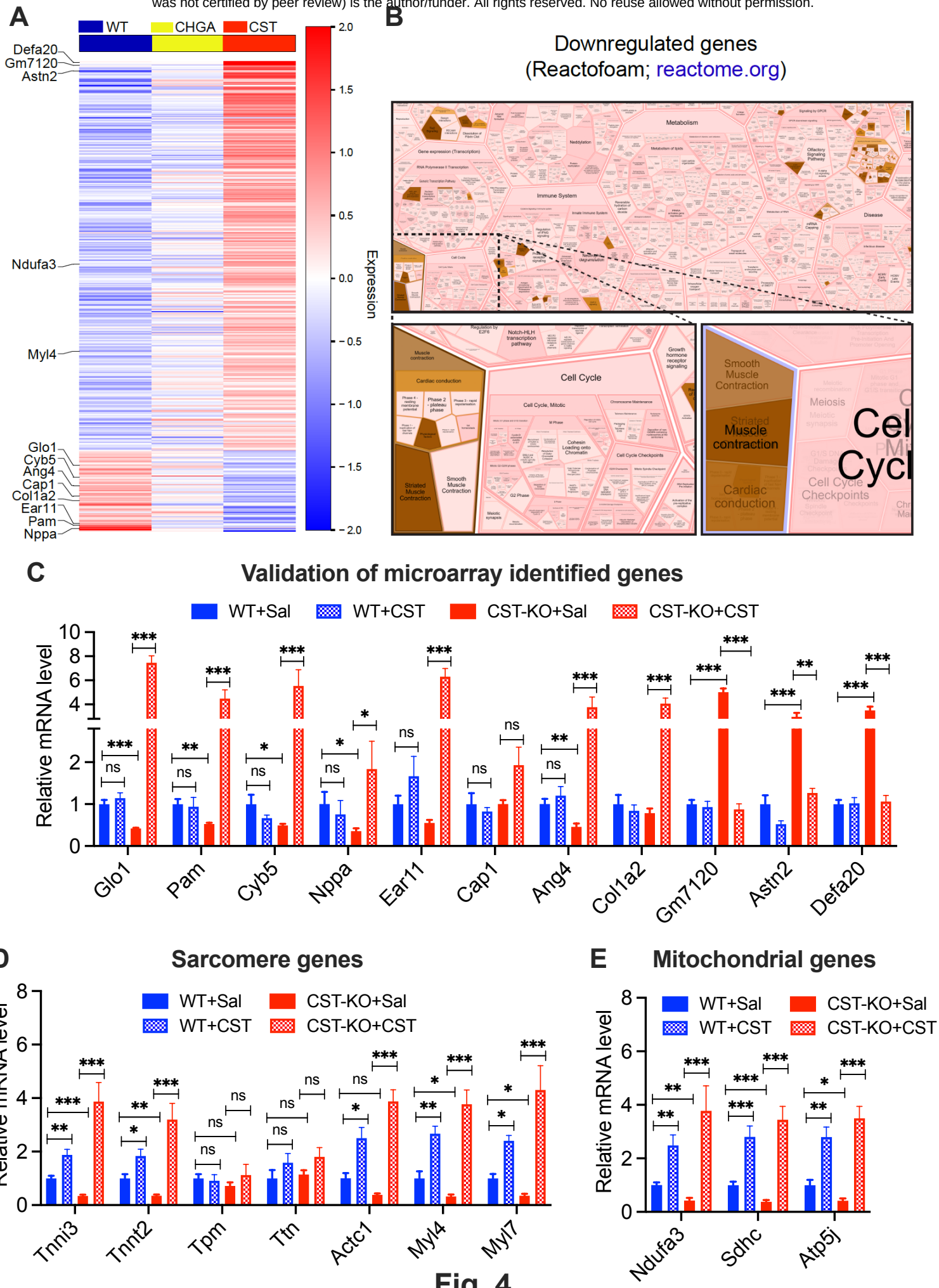

Fig. 4

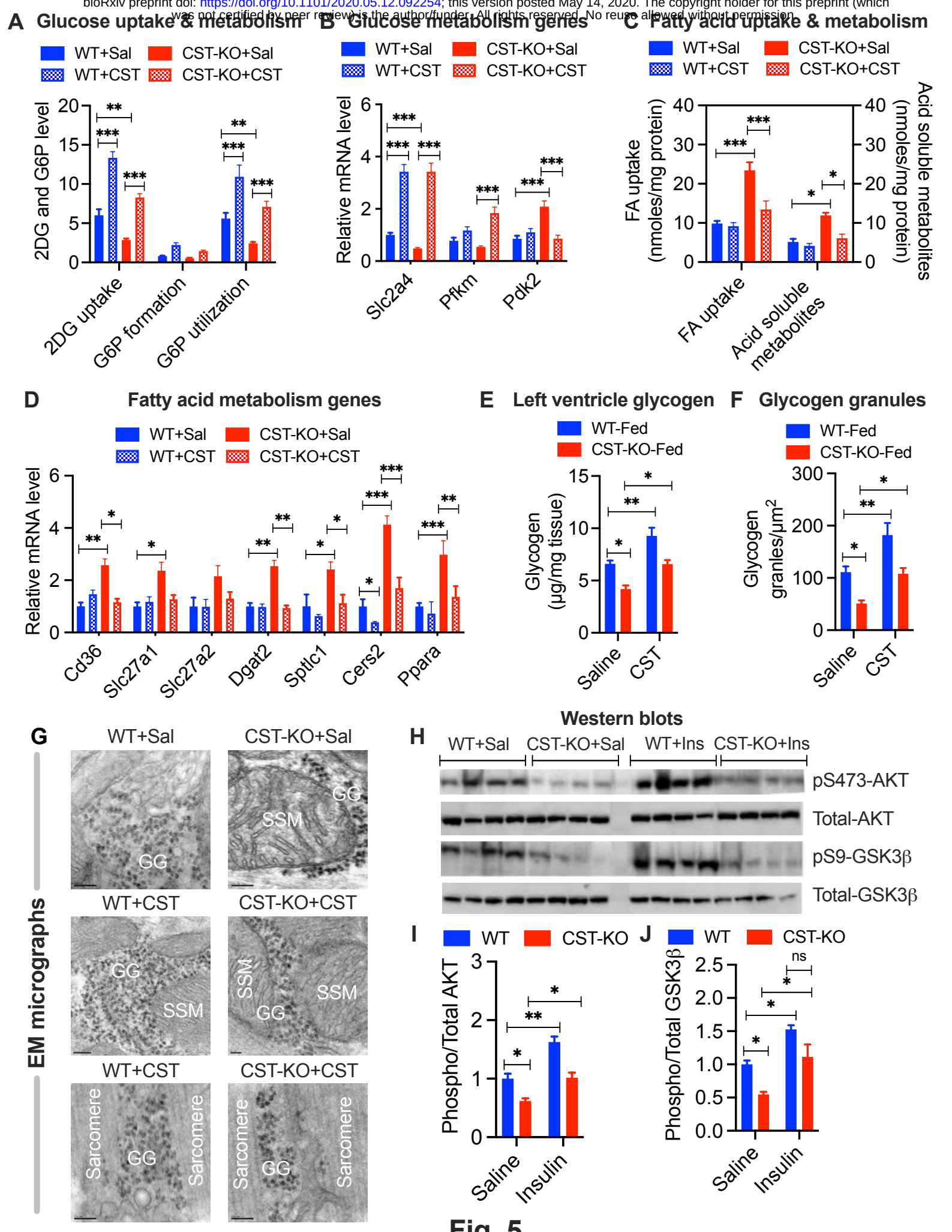

Fig. 5

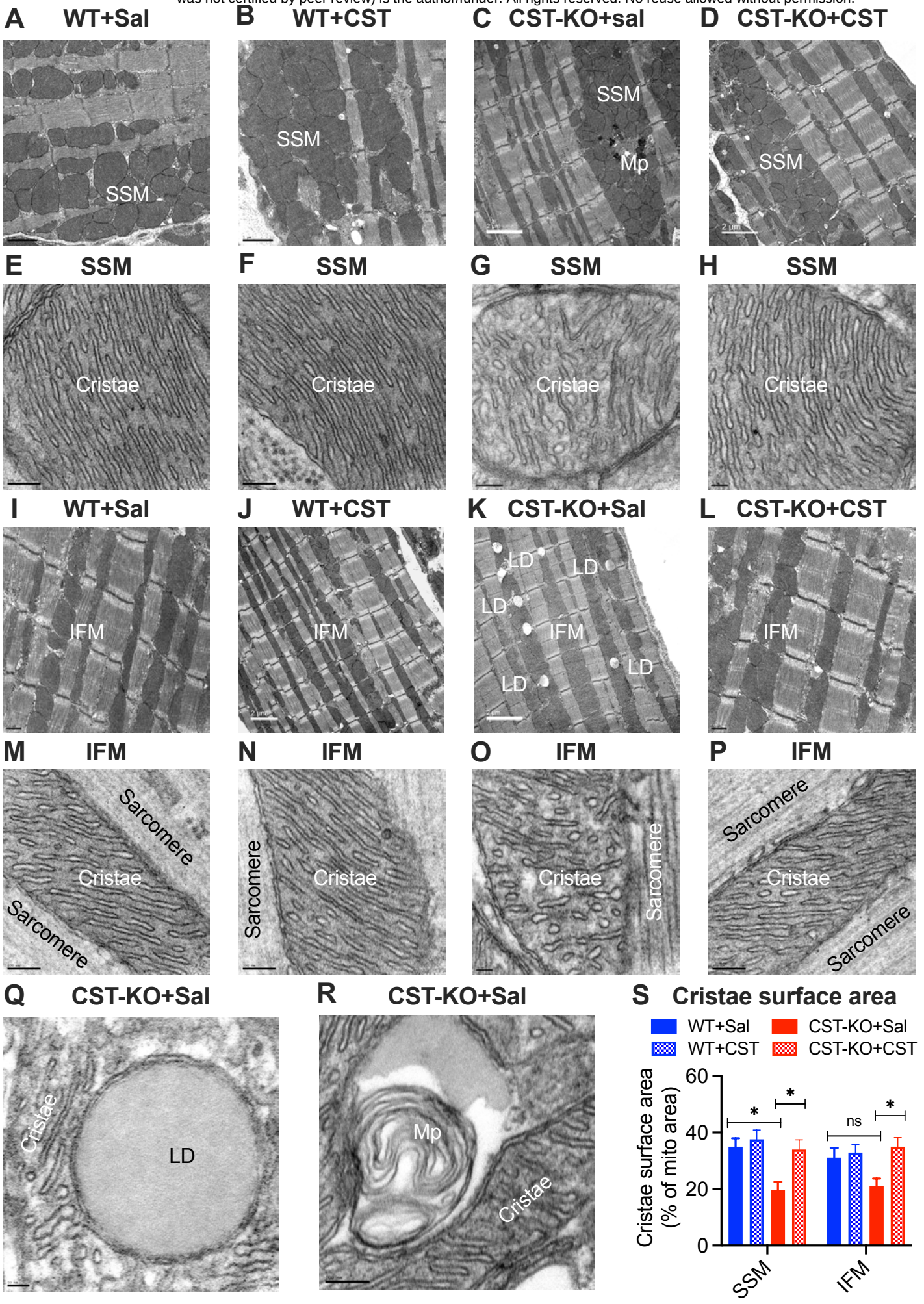

Fig. 6

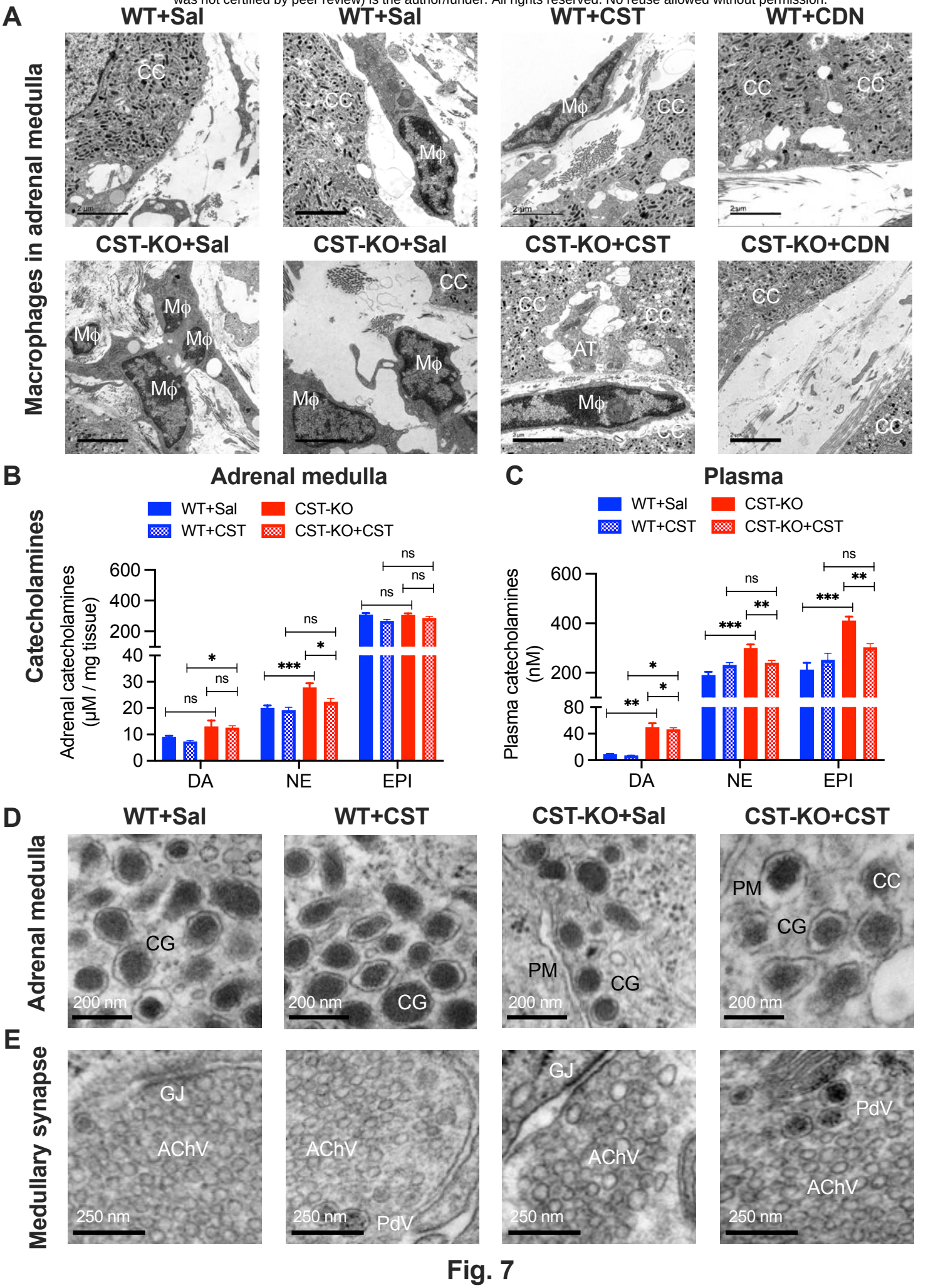

Fig. 7

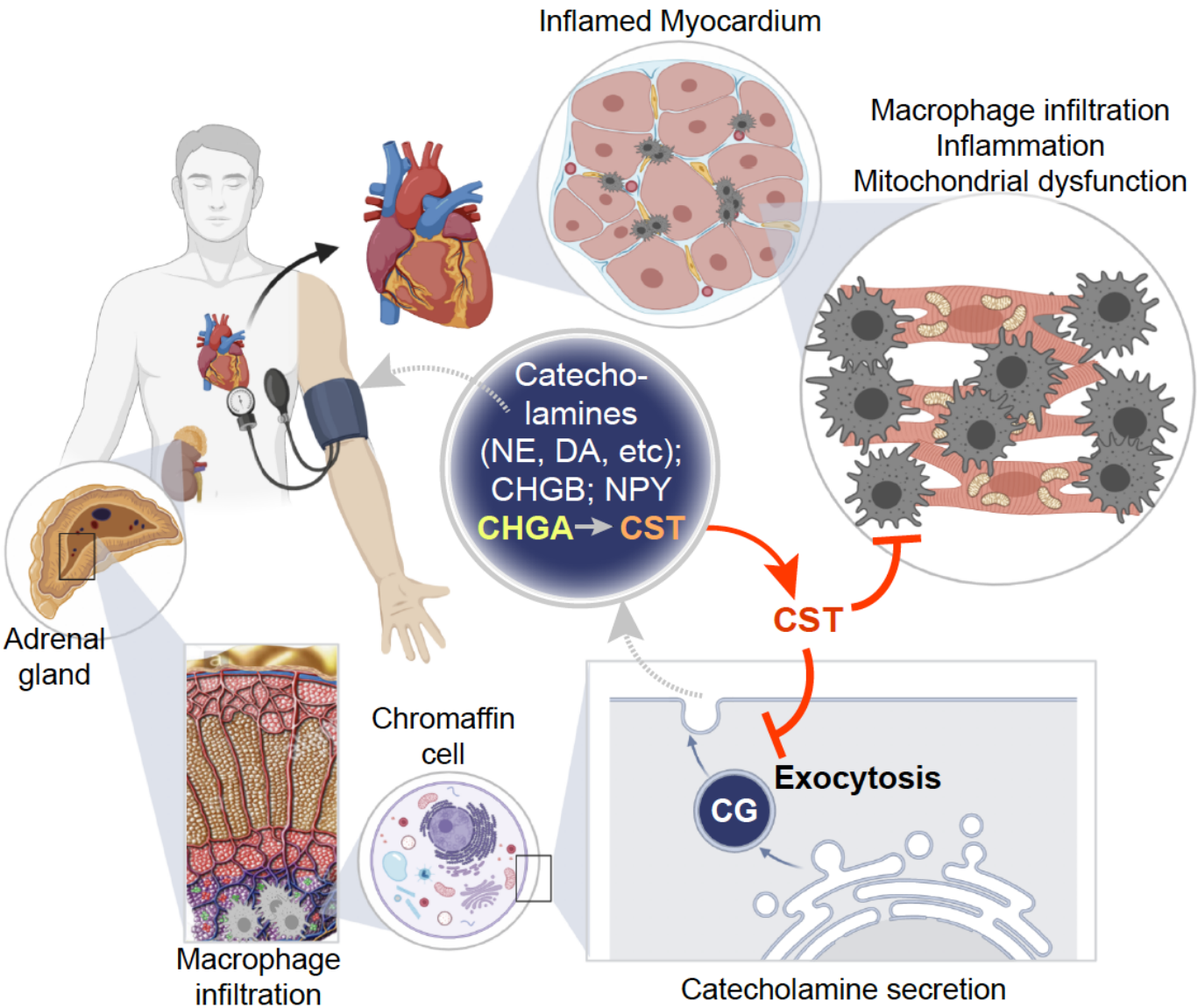
Inflamed Myocardium
Macrophage infiltration
Inflammation
Mitochondrial dysfunction
Catecho-
lamines
(NE, DA, etc);
CHGB; NPY
CHGA → CST
CST
Adrenal
gland
Chromaffin
cell
Exocytosis
CG
Macrophage
infiltration
Catecholamine secretion

Fig. 8

Supplemental Table S1. Primer sequences used in RT-qPCR experiments

Gene	Gene ID	Forward primer (5'-3')	Reverse primer (3'-5')
Actc1	11464	CTGGATTCTGGCGATGGTGTA	CGGACAATTTCACGTTCAGCA
Ang4	219033	GGTTGTGATTCCTCCAACTCTG	CTGAAGTTTTCTCCATAAGGGCT
Arg1	11846	CTCCAAGCCAAAGTCCTTAGAG	AGGAGCTGTCATTAGGGACATC
Astn2	56079	GCACAGCAGCGGACATTTC	TTCCTCAACGATCTCCGAGGG
Atp5j	11957	TATTGGCCCAGAGTATCAGCA	GGGGTTTGTCGATGACTTCAAAT
Cap1	12331	ATGGCTGACATGCAAAATCTTGT	TGGCAAGCAGCGAGTCAAAT
Ccl2	20296	TTAAAAACCTGGATCGGAACCAA	GCATTAGCTTCAGATTTACGGGT
Cd36	12491	ATGGGCTGTGATCGGAACTG	GTCTTCCCAATAAGCATGTCTCC
Cers2	76893	ATGCTCCAGACCTTGTATGACT	CTGAGGCTTTGGCATAGACAC
Clec10a	17312	TGAGAAAGGCTTTAAGAACTGGG	GACCACCTGTAGTGATGTGGG
Clec7a	56644	GACTTCAGCACTCAAGACATCC	TTGTGTCGCCAAAATGCTAGG
Col1a2	12843	GTAACTTCGTGCCTAGCAACA	CCTTTGTCAGAATACTGAGCAGC
Cxcl1	14825	CTGGGATTCACCTCAAGAACATC	CAGGGTCAAGGCAAGCCTC
Cyb5	109672	GGGCAGTCAGACAAGGATGTG	TCGTACACCTTATGATGCAGGA
Defa20	68009	TGTAGAAAAGGAGGCTGCAATAG	AGAACAAAAGTCGTCCTGAGC
Dgat2	67800	GCGCTACTTCCGAGACTACTT	GGGCCTTATGCCAGGAAACT
Ear11	93726	TGGAGCAACTTGAGTCTCGAC	CGGGGATAGGCTCTGTTATAGA
Emr1	13733	TGACTCACCTTGTGGTCCTAA	CTTCCCAGAATCCAGTCTTTCC
Glo1	109801	GATTTGGTCACATTGGGATTGC	TCCTTTCATTTTCCCGTCATCAG
Gm7120	633640	ACAGAATCCCTCATTTCCAGCA	CCGATCACTCCGTGTACTATGT
Ifng	15978	ATGAACGCTACACACTGCATC	CCATCCTTTTGCCAGTTCCTC
IL10	16153	GCTCTTACTGACTGGCATGA	CGCAGCTCTAGGAGCATGTG
IL12b	16160	TGGTTTGCCATCGTTTTGCTG	ACAGGTGAGGTTCACTGTTTCT
IL4	16189	GGTCTCAACCCCCAGCTAGT	GCCGATGATCTCTCTCAAGTGAT
Itgam	16409	CCATGACCTTCCAAGAGAATGC	ACCGGCTTGTGCTGTAGTC
Itgax	16411	CTGGATAGCCTTTCTTCTGCTG	GCACACTGTGTCCGAACTCA
Mrc1	17533	CTCTGTTCAGCTATTGGACGC	CGGAATTTCTGGGATTCAGCTTC
Myl4	17896	AAGAAACCCGAGCCTAAGAAGG	TGGGTCAAAGGCAGAGTCCT
Myl7	17898	GGCACAACGTGGCTCTTCTAA	TGCAGATGATCCCATCCCTGT
Ndufa3	66091	ATGGCCGGGAGAATCTCTG	AGGGGCTAATCATGGGCATAAT
Nos2	18126	GTTCTCAGCCCAACAATACAAGA	GTGGACGGGTCGATGTCAC
Nppa	230899	GCTTCCAGGCCATATTGGAG	GGGGGCATGACCTCATCTT
Pam	18484	CTGGGGTCACACCTAAAGAGT	ATGAGGGCATGTTGCATCCAA
Pdk2	18604	AGGGGCACCCAAGTACATC	TGCCGGAGGAAAGTGAATGAC
Pfkm	18642	TGTGGTCCGAGTTGGTATCTT	GCACTTCCAATCACTGTGCC
Ppara	19013	AGAGCCCCATCTGTCCTCTC	ACTGGTAGTCTGCAAAACCAAA
Sdhc	66052	GCTGCGTTCTTGCTGAGACA	ATCTCCTCCTTAGCTGTGGTT

Slc27a1	26457	CGCTTTCTGCGTATCGTCTG	GATGCACGGGATCGTGTCT
Slc27a2	26458	TCCTCCAAGATGTGCGGTACT	TAGGTGAGCGTCTCGTCTCG
Slc2a4	20528	GTGACTGGAACACTGGTCCTA	CCAGCCACGTTGCATTGTAG
Sptlc1	268656	ACGAGGCTCCAGCATACCAT	TCAGAACGCTCCTGCAACTTG
Tnf	21926	CCCTCACACTCAGATCATCTTCT	GCTACGACGTGGGCTACAG
Tnni3	21954	TCTGCCAACTACCGAGCCTAT	CTCTTCTGCCTCTCGTTCCAT
Tnnt2	21956	CAGAGGAGGCCAACGTAGAAG	CTCCATCGGGGATCTTGGGT
Tpm1	22003	CAGAAGGCAAATGTGCCGAG	TCCAGCATCTGGTGCATACTA
Ttn	22138	GACACCACAAGGTGCAAAGTC	CCCACTGTTCTTGACCGTATCT

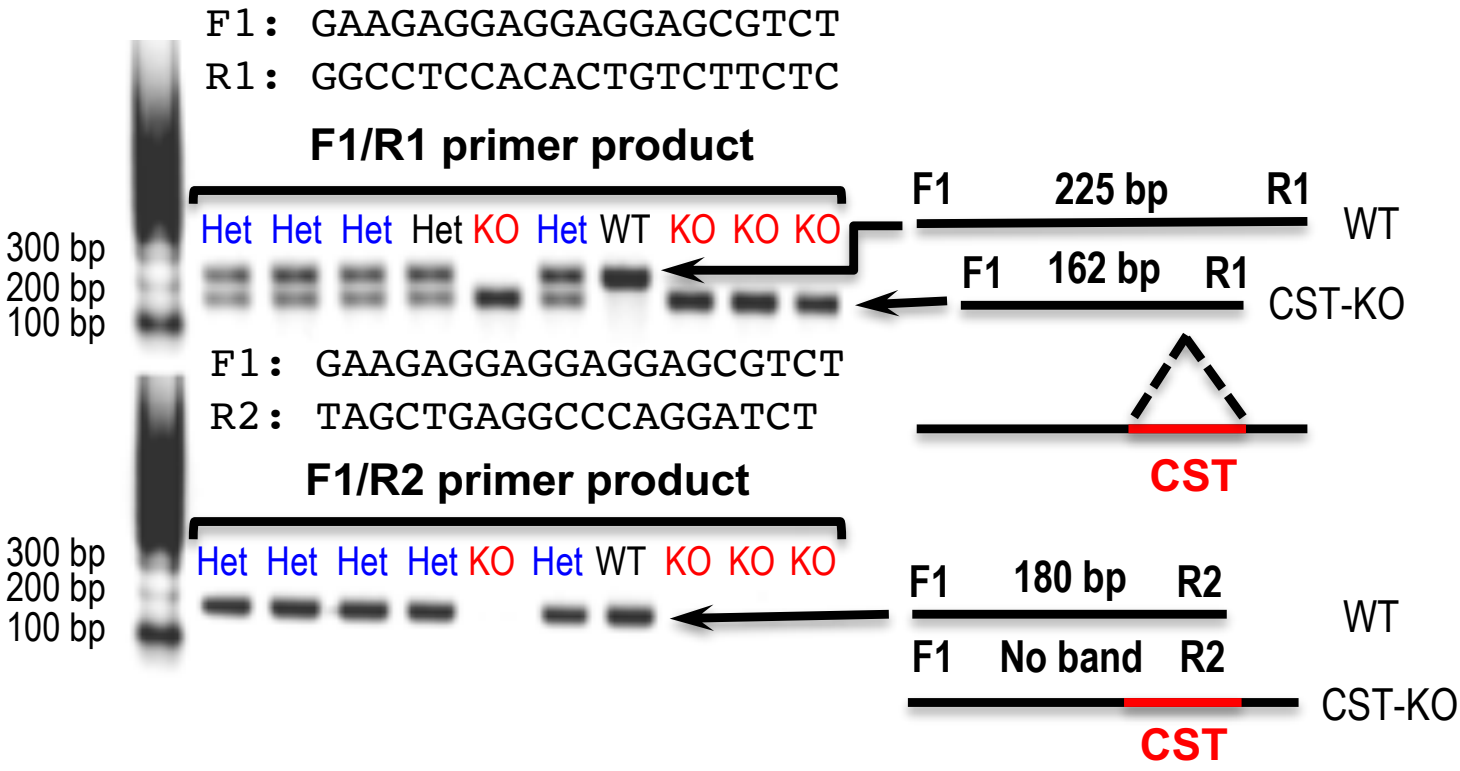
F1: GAAGAGGAGGAGGAGCGTCT
R1: GGCCTCCACACTGTCTTCTC
F1/R1 primer product
Het Het Het Het KO Het WT KO KO KO
300 bp
200 bp
100 bp
F1 225 bp R1
WT
F1 162 bp R1
CST-KO
F1: GAAGAGGAGGAGGAGCGTCT
R2: TAGCTGAGGCCCAGGATCT
CST
F1/R2 primer product
Het Het Het Het KO Het WT KO KO KO
300 bp
200 bp
100 bp
F1 180 bp R2
WT
F1 No band R2
CST-KO
CST

Fig. S1

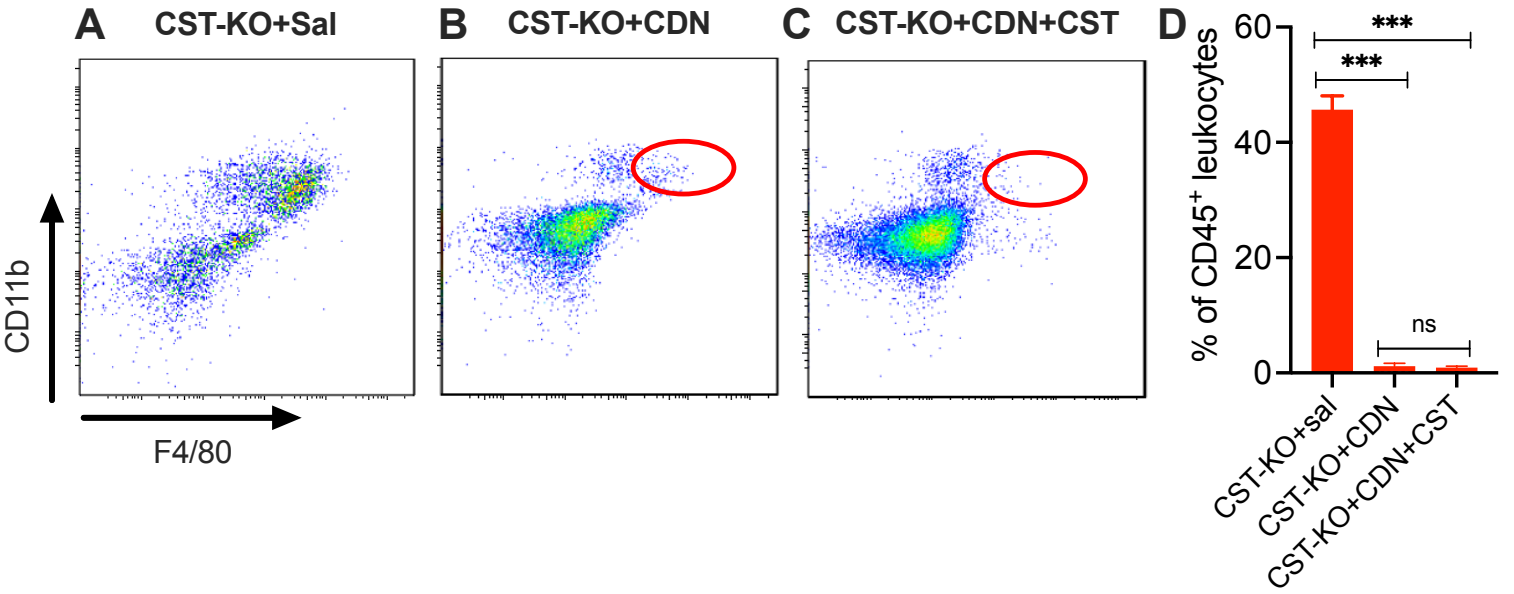
A
CST-KO+Sal
B
CST-KO+CDN
C
CST-KO+CDN+CST
D
CD11b
F4/80
% of CD45+ leukocytes
60
40
20
0
***
***
ns
CST-KO+sal
CST-KO+CDN
CST-KO+CDN+CST

Fig. S2

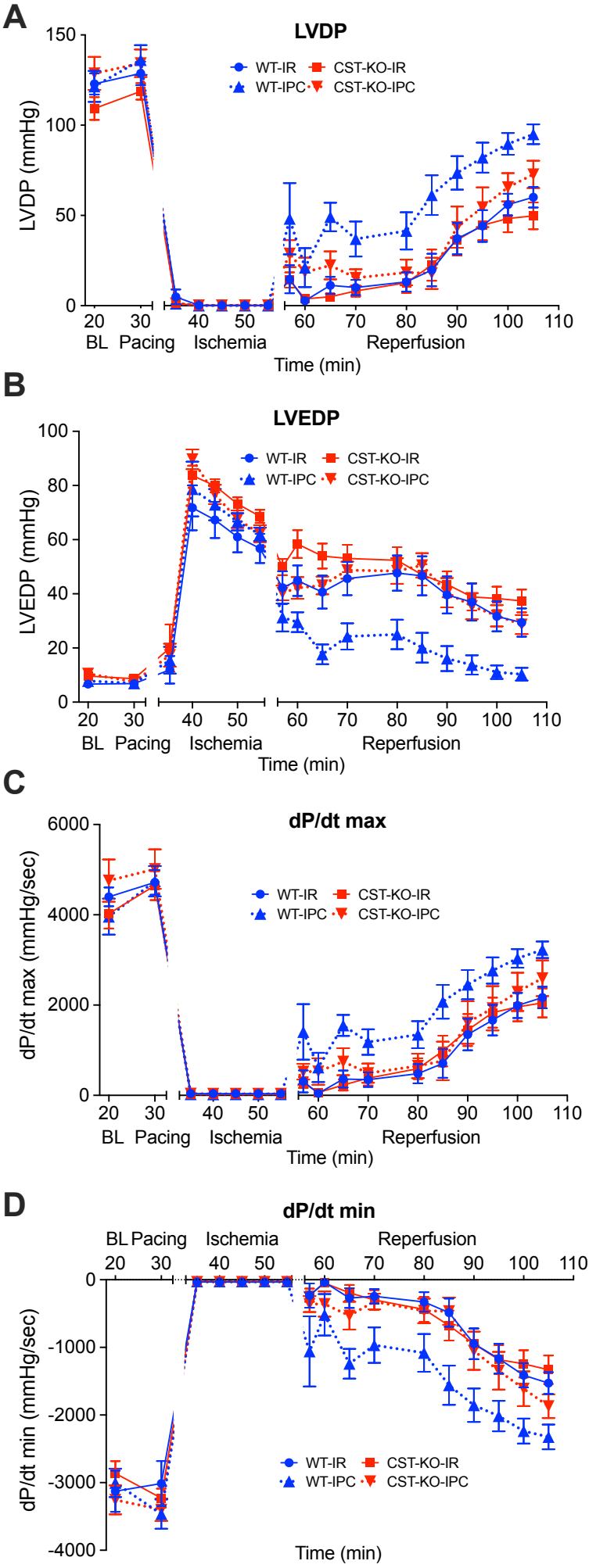
A
LVDP
WT-IR
CST-KO-IR
WT-IPC
CST-KO-IPC
LVDP (mmHg)
150
100
50
0
20
30
40
50
60
70
80
90
100
110
BL
Pacing
Ischemia
Reperfusion
Time (min)
B
LVEDP
WT-IR
CST-KO-IR
WT-IPC
CST-KO-IPC
LVEDP (mmHg)
100
80
60
40
20
0
20
30
40
50
60
70
80
90
100
110
BL
Pacing
Ischemia
Reperfusion
Time (min)
C
dP/dt max
WT-IR
CST-KO-IR
WT-IPC
CST-KO-IPC
dP/dt max (mmHg/sec)
6000
4000
2000
0
20
30
40
50
60
70
80
90
100
110
BL
Pacing
Ischemia
Reperfusion
Time (min)
D
dP/dt min
BL
Pacing
Ischemia
Reperfusion
20
30
40
50
60
70
80
90
100
110
0
-1000
-2000
-3000
-4000
dP/dt min (mmHg/sec)
WT-IR
CST-KO-IR
WT-IPC
CST-KO-IPC
Time (min)

Fig. S3